

Acta Geodaetica et Geophysica

The role of pargasitic amphibole in the formation of major geophysical discontinuities in the shallow upper mantle --Manuscript Draft--

Manuscript Number:	
Full Title:	The role of pargasitic amphibole in the formation of major geophysical discontinuities in the shallow upper mantle
Article Type:	Original Study
Section/Category:	Acta Geodaetica Issue
Keywords:	lithosphere-asthenosphere boundary (LAB); mid lithosphere discontinuities (MLD); amphibole; melt; water
Corresponding Author:	Istvan Janos Kovacs, PhD Geological and Geophysical Institute of Hungary Budapest, HUNGARY
Corresponding Author's Institution:	Geological and Geophysical Institute of Hungary
First Author:	Istvan Janos Kovacs, PhD
Order of Authors:	Istvan Janos Kovacs, PhD László Lenkey, PhD David H. Green Tamás Fancsik György Falus János Kiss László Orosz Zsuzsanna Viktor Jolán Angyal
Funding Information:	Bolyai Postdoctoral Fellowship Dr. Istvan Janos Kovacs
Abstract:	<p>Several explanations have been proposed for variation in geophysical properties and depths to the lithosphere-asthenosphere boundary (LAB) and mid-lithospheric discontinuities (MLD). Here we investigate the proposal that the dehydration solidus of pargasitic amphibole-bearing upper mantle with very low bulk water (hundreds ppm) may be one of the main reasons for the observed geophysical anomalies. The pargasite dehydration solidus may be associated with a very small degree of partial melting in the upper mantle at temperatures and pressures in excess of 1050 °C (for geochemically more depleted) or 1100 °C (for geochemically more fertile upper mantle) and from 1 to 3 GPa (~ 30 to 90 km) respectively. This small amount of partial melt may be responsible for changes in geophysical properties (e.g. lower seismic velocity, higher attenuation of seismic waves, higher electrical conductivity) in association with the LAB and MLD. This simple petrologic model is tested on the abundant geophysical data of the Carpathian-Pannonian region (CPR), central Europe. The high resolution heat flow data available in the CPR allows us to estimate the depths to intersection of area specific depth-temperature curves with the dehydration solidus temperatures (1050 and 1100 °C isotherms). There is relatively small mismatch (< 5 km) between the position of these intersections and the geophysically determined LAB in the central area of the CPR. These observations lend support for the proposition that the dehydration solidus may be largely responsible for depth variation of the LAB in young continental rift areas. Towards the margins of the CPR, however, where the heat flow is lower (< ~ 70 mW/m²), the predictive capability of the dehydration solidus model deteriorates. This is because, for lower geothermal gradients, pargasitic amphibole breaks down at ~90 km (or ~ 3 GPa) before temperature exceeds the dehydration solidus temperatures. Consequently we should expect changes in geophysical</p>

	<p>properties attributable to hydrous silicate melt at ~90 km depth in areas where surface heat flow is lower (i.e. Precambrian cratonic shields, Phanerozoic continental lithospheres or, possibly older oceanic plates). Alternatively, in these areas, the intersection of the geotherm with pargasite breakdown may correlate with the MLD rather than the LAB, which is at deeper levels.</p>
<p>Suggested Reviewers:</p>	<p>Sierd A.P.L. Cloetingh, PhD Professor, Utrecht University S.A.P.L.Cloetingh@uu.nl Sierd is a widely acknowledged expert of tectonic and rheological behaviour of the lithosphere</p> <hr/> <p>Antal Embey-Isztin, DSc retired senior research fellow, Hungarian Mudeum for Natural Sciences embey@ludens.elte.hu A widely recognized expert of the upper mantle and its geochemistry beneath the Carpathian-Pannonian Region</p> <hr/> <p>Gábor Dobosi, DSc Professor, University of Debrecen dobosi@geochem.hu A great expert of the upper mantle beneath the Carpathian-Pannonian Region</p> <hr/> <p>Karoly Hidas, PhD Postdoctoral Fellow, Spanish NAtional Reserach Council karoly.hidas@gmail.com Expert of deformation and kinematisic of the lithosphere</p>

The role of pargasitic amphibole in the formation of major geophysical discontinuities in the shallow upper mantle

István, Kovács^{1*}, László, Lenkey², David. H. Green³, Tamás, Fancsik¹, György, Falus¹, János Kiss¹, László, Orosz¹, Jolán Angyal¹, Zsuzsanna Viktor¹

1) Geological and Geophysical Institute of Hungary, Stefánia street 14., Budapest, Hungary

2) Department of Geophysics, Eötvös University, Pázmány Péter street 1/C, 1117, Budapest, Hungary

3) University of Tasmania, Hobart, Australia

* corresponding author: kovacs.istvan.janos@mfgi.hu

Abstract

Several explanations have been proposed for variation in geophysical properties and depths to the lithosphere-asthenosphere boundary (LAB) and mid-lithospheric discontinuities (MLD). Here we investigate the proposal that the *dehydration solidus* of pargasitic amphibole-bearing upper mantle with very low bulk water (hundreds ppm) may be one of the main reasons for the observed geophysical anomalies. The pargasite *dehydration solidus* may be associated with a very small degree of partial melting in the upper mantle at temperatures and pressures in excess of 1050 °C (for geochemically more depleted) or 1100 °C (for geochemically more fertile upper mantle) and from 1 to 3 GPa (~ 30 to 90 km) respectively. This small amount of partial melt may be responsible for changes in geophysical properties (e.g. lower seismic velocity, higher attenuation of seismic waves, higher electrical conductivity) in association with the LAB and MLD. This simple petrologic model is tested on the abundant geophysical data of the Carpathian-Pannonian region (CPR), central Europe. The high resolution heat flow data available in the CPR allows us to estimate the depths to intersection of area specific depth-temperature curves with the *dehydration solidus* temperatures (1050 and 1100 °C isotherms). There is relatively small mismatch (< 5 km) between the position of these intersections and the geophysically determined LAB in the central area of the CPR. These observations lend support for the proposition that the *dehydration solidus* may be largely responsible for depth variation of the LAB in young continental rift areas. Towards the margins of the CPR, however, where the heat flow is lower (< ~ 70 mW/m²), the predictive

1 capability of the *dehydration solidus* model deteriorates. This is because, for lower
2 geothermal gradients, pargasitic amphibole breaks down at ~90 km (or ~ 3 GPa) before
3 temperature exceeds the *dehydration solidus* temperatures. Consequently we should expect
4 changes in geophysical properties attributable to hydrous silicate melt at ~90 km depth in
5 areas where surface heat flow is lower (i.e. Precambrian cratonic shields, Phanerozoic
6 continental lithospheres or, possibly older oceanic plates). Alternatively, in these areas, the
7 intersection of the geotherm with pargasite breakdown may correlate with the MLD rather
8 than the LAB, which is at deeper levels.
9
10
11
12
13
14
15

16 Keywords: lithosphere-asthenosphere boundary (LAB), mid lithosphere discontinuities
17 (MLD), amphibole, melt, water
18
19
20
21

22 **Introduction**

23
24

25 The lithosphere-asthenosphere boundary (LAB) is one of the most fundamental
26 discontinuities in the Earth's interior separating the outer, rigid lithosphere from the
27 convective and more plastic asthenosphere underneath. The classic view of plate tectonics is
28 that the rigid but fragmented outer shell (lithosphere) floats on the less viscous asthenosphere
29 with relative plate movements driven by ridge push, subduction pull and active asthenospheric
30 flows or the combination of these forces. The LAB is thus a rapid change of viscosity over a
31 small depth interval and such a rheological change cannot be sensed directly by geophysical
32 techniques. However seismic velocities, seismic attenuation and electrical conductivity can be
33 measured and layers showing generally lower seismic velocity, greater seismic attenuation
34 and higher electrical conductivity are commonly assumed to equate with the asthenosphere.
35 With this simplifying and reasonable assumption, the LAB represents the uppermost part of
36 the global low velocity zone which extends from the LAB to the Lehman boundary at ~220
37 km depth (Fischer et al. 2010). Yet more than 100 years from the early theory of continental
38 drift (Wegener 1912; Carey 1958), and more than 50 years after the birth of the modern
39 theory of plate tectonics (Dietz 1961; Wilson 1963; Mason and Raff 1961) there is still no
40 consensus as to what causes the weakening at the LAB and whether the seismological and
41 electrical discontinuities/layers should be equated to the rheological boundaries. In addition,
42 there is still an ongoing controversy how LAB is related to sometimes multiple discontinuities
43 found in cratonic and thicker continental lithospheres (i.e. mid-lithosphere discontinuities
44 referred to as MLD(s) hereafter) (i.e., Thybo 2006; Abt et al. 2010; Selway et al. 2015; Karato
45
46
47
48
49
50
51
52
53
54
55
56
57
58
59
60
61
62
63
64
65

1 et al. 2015). As well as rheological, seismological and electro-magnetic properties of the
2 upper mantle, thermal/heat-flow and density/gravity observations must also be reconciled
3 with mineralogical and petrological characteristics of inferred or sampled upper mantle
4 compositions. Heat-flow and inferred geothermal gradients are particularly important in their
5 relationship to melting in the mantle and as sensors for thermal perturbations in plate tectonics
6 (McKenzie 1978; McKenzie & Bickle 1988).
7
8
9

10 It is not our primary aim here to give a very comprehensive overview of processes that
11 have been already invoked to explain the rheological weakening and geophysical properties
12 characteristic for the LAB and MLD. Instead, after a brief discussion of these proposals, we
13 test the application of a petrological model involving the stability of pargasitic amphibole (i.e.
14 Green 1971; 1973; Green and Liebermann 1976; Green 2015) and solidi of lherzolitic mantle,
15 containing very small water (and carbon) contents. For this we will include heat flow, seismic
16 and magnetotelluric (i.e. Horváth 1993; Posgay et al. 1995; Tari et al. 1999; Horváth et al.
17 2006) data with dense areal coverage from the Carpathian Pannonian region, central Europe
18 (CPR), which is an excellent ‘natural laboratory’ to test this petrologic model, as suggested by
19 McKenzie (1978).
20
21
22
23
24
25
26
27
28
29

30 **Theoretical Background**

31
32
33
34 *Overview on petrologic models for the LAB based on high pressure experimental study of the*
35 *mineralogy and melting relations of mantle peridotite*
36
37
38
39

40 *‘Hydrolytic weakening’*

41 Olivine (Mg# ~ 90) and pyroxenes (orthopyroxene > clinopyroxene) are the dominant
42 minerals stable in uppermost mantle lherzolite compositions and much effort has been applied
43 to determining the physical properties of these minerals as functions of pressure and
44 temperature. Studies have demonstrated the presence of trace water in defect sites in olivine
45 and pyroxenes, which are nominally anhydrous minerals (NAMs, i.e., Smyth et al. 1991; Bell
46 and Rossman 1992). It has been argued that trace water in olivine and pyroxenes as structural
47 hydroxyl in particular sites causes ‘hydrolytic weakening’ (Kohlstedt et al. 1996; Hirth and
48 Kohlstedt 1996). If the lithosphere has lower water contents because of melt extraction at
49 mid-ocean ridges, the residual depleted peridotite approaches an anhydrous state and thus
50 becomes high strength lherzolite to harzburgite. The inferred higher concentration of ‘water’
51 in the undepleted asthenosphere leads to ‘hydrolytic weakening’ of the mineral structures
52
53
54
55
56
57
58
59
60
61
62
63
64
65

1 causing lower seismic velocities and higher seismic attenuation. In addition, the elevated
2 'water' contents of NAMs contribute to the higher electric conductivity. In this interpretation,
3 the asthenosphere and lithosphere are both subsolidus but differ in water content in olivine
4 and pyroxenes. No significance is attached to pargasite stability. In addition a recent
5 experimental study demonstrated that the weakening of mineral structures due to the
6 incorporation of 'water' in NAMs as structural hydroxyl may not be significant. (Girard et al.
7 2013).

14 *Elastically accommodated grain boundary sliding*

16 Elastically accommodated grain boundary sliding (EAGBS for short; i.e., Karato 2013;
17 Karato et al. 2015) has also been proposed as the main mechanism for changes seen in
18 mineral properties at the LAB. This theory implies that at moderate temperatures grain
19 boundaries weaken, thus, grain boundary sliding facilitated by elastic deformation of grains
20 can occur. Consequently during the transition from elastic to anelastic behavior with
21 increasing temperatures there is a point when EAGBS takes place. This produces a
22 temperature and frequency-dependent band in seismic attenuation. The lowering of the elastic
23 modulus results in lower seismic velocities of polycrystalline aggregates, such as mantle
24 peridotites. Experimental studies, however, demonstrated that EAGBS may be very sensitive
25 to grain size, 'water' content in NAMs and modal compositions of mantle peridotites. The
26 effects of these factors are only poorly constrained, creating uncertainty in P-T conditions
27 under which EAGBS is effective. Calculations involving the currently available experimental
28 data indicate that the temperature at which EAGBS occurs is most probably at ~900-1000 °C
29 (Faul and Jackson 2005; Jackson et al. 2014; Karato et al. 2015). This is very similar to the
30 water-saturated solidus of pargasite-bearing lherzolite (*water-saturated solidus* is 980 – 1025
31 °C from 1.5 – 2.5 GPa, **Fig. 1**), and also overlaps the solidus for carbonatite melt (930 °C at 2
32 GPa; Green, 2015). Thus, while EAGBS can be considered as a potential mechanism for
33 influencing mineral properties at the LAB (or MLDS), its distinction from the effects of
34 partial melting may be difficult.

35 Besides the models summarized above several other explanations such as
36 compositional layering and variations in the geometry of seismic anisotropy in the upper
37 mantle may explain the observed seismic anomalies. Selway et al. (2015), however, proposed
38 – based on a summary of natural xenoliths - that these factors could only act on a local scale
39 and may not explain the global presence of major discontinuities such as the LAB or MLD.
40
41
42
43
44
45
46
47
48
49
50

Partial melting and the role of pargasite

1 An alternative to these hypotheses is that the lithosphere is subsolidus but with increasing
2 temperature along the geotherm (i.e. depth-temperature curve), the solidus of mantle
3 peridotite is crossed (and the intersection equates to the LAB) and the asthenosphere has
4 interstitial melt present. The presence of a small amount (maximum ~ 1 – 2 wt.% but typically
5 significantly less) of partial melt causes the changes in geophysical properties associated with
6 the LAB and MLD. While there is a general agreement that a small amount of partial melt
7 could significantly reduce seismic velocities (Kawakatsu et al. 2009; Takei and Holtzman
8 2009), increase conductivity (Ni et al. 2011) and seismic attenuation (Hammond and
9 Humphreys 2000), it is debated whether even small degree of partial melting could occur
10 under conditions prevailing in the vicinity of the LAB and MLD (Karato et al. 2015).

11 The amphibole, pargasite, is found in natural lherzolites, including lithospheric mantle
12 sampled from slow-spreading ridges and fracture zones, and peridotite xenoliths from
13 kimberlites and silica-undersaturated primary basalts (i.e. Griffin et al. 1984; Konzett et al.
14 2000; Szabó et al. 2004). Pargasite contains essential Na₂O and TiO₂ and from 1.5 to 2 wt.%
15 H₂O and its stability in lherzolitic compositions is well determined experimentally as a
16 function of pressure, temperature and composition (enriched, fertile and depleted lherzolite
17 compositions; Green 1973; Wallace & Green 1991; Niida & Green 1999; Green et al. 2014).
18 In a model mantle (see Green et al. 2014 and Green 2015 for details) the pargasite
19 composition and modal abundance are controlled by P, T and water content, and pargasite
20 may form up to 25 wt.% at ~ 1000 °C and 1 - 2 GPa (Niida & Green 1999) in fertile
21 compositions (MPY, HZ lherzolites) or enriched compositions (HPY). Most importantly, at
22 lithospheric pressures, pargasite is stable up to 3 GPa and three distinctive solidi must be
23 considered (Green et al. 2010; Green 2015; see **Fig. 1** for an overview):

- 24 (i) the *water-saturated solidus* if the water content exceeds the storage capacity
25 defined by the modal pargasite and NAMs (> ~0.4 wt.%) at pressures < 3 GPa., or
26 the storage capacity of NAMs (> ~ 190 ppm) at > 3 GPa.
- 27 (ii) the (*pargasite*) *dehydration solidus* if water content exceeds that which can be
28 stored in NAMs (> ~ 190 ppm) but is less than the storage capacity defined by the
29 modal pargasite and NAMs (< ~0.4 wt.%) at pressures < 3 GPa.
- 30 (iii) the solidus with bulk water content less than that which can be stored in NAMs (<
31 ~ 190 ppm), thus approaching the *anhydrous solidus*.

1
2 The important role of pargasite in defining the dehydration solidus in the uppermost
3 mantle, despite being crucial, has been generally overlooked or omitted possibly because of:
4 1) unfamiliarity with the amphibole: pargasite and its role in the lherzolite phase equilibria; 2)
5 unawareness on the roles of minor components (i.e. Na, Ti, K) in stabilizing pargasite or
6 phlogopite to high temperature at upper mantle conditions; 3) ignorance of the roles which
7 extremely incompatible elements (such as H, K, P, and C) have in introducing additional rare
8 subsolidus minerals and in lowering solidus temperatures (i.e., ‘fluxing’ melting); 4)
9 unfamiliarity with the role of ‘incipient melting’ in fertile or enriched lherzolite. A very small
10 melt fraction, enriched in volatile and highly incompatible components, is present over a large
11 temperature interval, until temperature approaches the *anhydrous solidus* (**Fig. 1**) for an upper
12 mantle lacking C-H-O vapour or highly incompatible element-rich phases; 5) paucity of data
13 on the rheological, seismological and electrical conductivity effects of extremely small melt
14 fractions of hydrous silicate melts, including their distribution and porosity/permeability
15 effects.
16
17
18
19
20
21
22
23
24
25
26

27 *The importance of the pargasite-based petrological model*

28
29
30

31 In the petrological model adopted here including the role of pargasitic amphibole LAB is
32 interpreted as the high pressure or temperature limit of pargasite stability so that the geotherm
33 passed from subsolidus pargasite-bearing lherzolite to pargasite-free lherzolite with a small
34 melt fraction (< 1 wt %; **Fig 1**). Consequently the asthenosphere is a layer with incipient
35 melting, the melt fraction being controlled by the volatile components, particularly H₂O
36 (Lambert & Wyllie 1970; Green 1971; 1973; Green & Liebermann 1976).
37
38
39
40
41

42 It is not surprising that, without taking into account the role of pargasite and the
43 *dehydration solidus* (**Fig 1**), it has remained challenging to explain the existence of a small
44 melt fraction in the shallow upper mantle at the LAB or MLD. This is because the *anhydrous*
45 *solidus* temperature of shallow upper mantle peridotite increases almost linearly from ~1100
46 °C at ambient pressure to ~1500 °C at 3 GPa (**Fig. 1**). *Anhydrous solidus* temperatures
47 generally exceed, at least by 200 °C, those typical for a normal intra-plate geotherm at a given
48 depth (**Fig. 1**). Thus, partial melting of dry upper mantle peridotite could not explain the
49 presence of a small amount of partial melt at the LAB or MLD.
50
51
52
53
54
55

56 Theoretical models on the effect of several hundred to thousands ppm of water in
57 nominally anhydrous minerals (NAMs) in lherzolite (Katz et al. 2003; Hirschmann 2009)
58 predicted decrease of the solidus temperature of mantle peridotite to intersect geotherms as in
59
60
61
62
63
64
65

1
2
3
4
5
6
7
8
9
10
11
12
13
14
15
16
17
18
19
20
21
22
23
24
25
26
27
28
29
30
31
32
33
34
35
36
37
38
39
40
41
42
43
44
45
46
47
48
49
50
51
52
53
54
55
56
57
58
59
60
61
62
63
64
65

Fig. 1. These models disregarded the role of pargasite. Katz et al. (2003) argued that the presence of 500 and 1000 ppm bulk water reduces the *anhydrous solidus* temperature by ~ 150 and 200 °C respectively at a given pressure (**Fig. 1**). In this model, one would need at least 1000 ppm water generally in the shallow upper mantle to intersect the intra-plate geotherm at depths characteristic for the LAB or MLD (**Fig. 1**). Such large amount of bulk water, however, is inconsistent with our present knowledge on the average storage capacity for water in the Earth's upper mantle. Experimental works as well as studies on natural upper mantle peridotites revealed that normal MORB-source upper mantle contains only ~ 50 - 200 ppm water (Michael 1988; 1995; Danyushevsky et al. 2000; Saal et al. 2002; Green et al. 2010; Peslier 2010; Kovács et al. 2012; Warren and Hauri 2014; Demouchy and Bolfan-Casanova 2016; Xu et al. 2016). This is significantly less than what would be needed (~ 1000 ppm) in the Katz et al. (2003) model to intersect intra plate geotherms and initiate partial melting in the shallow upper mantle (Fig. 1). Only OIB, enriched-MORB and island arc upper mantle sources appear to acquire up to 300 – 1000 ppm water (Dixon et al. 2002; Hauri et al. 2002; Asimow et al. 2004) but their localized appearance could not explain the global presence of the LAB or MLDs. Intersection of geotherms with the *water saturated solidus* of fertile mantle predicts partial melt at ~75 km in the upper mantle, or at greater depths for cooler geotherms (**Fig. 1**). At depths less than ~ 90 km, more than 0.4 wt.% bulk water is necessary for water saturation in fertile lherzolite (i.e. exceeding the water storage capacity of pargasite lherzolite). Such high water contents may only be present in the immediate vicinity of subduction zones. In intraplate locations it is the *dehydration solidus* which is relevant.

Intersection of model geotherms with the (pargasite) *dehydration solidus* predicts partial melt at < 90 km only in areas of high heat-flow. The depth of the intersections increases with decreasing heat flow to a 'critical' or 'optimal' heat-flow. This is the expected behaviour of aging oceanic lithosphere at increasing distance from a mid-ocean ridge. It is also the expected behaviour for thermal relaxation from a perturbed geotherm caused by lithospheric thinning, rifting, asthenospheric upwelling, and intraplate basaltic volcanism. The perturbed heat-flow approaches the pre-rifting or steady state value. At the 'critical' heat flow, the geotherm intersects the solidus at the inflexion from $dT/dP \sim 0$ to negative value. In **Fig 2** this 'critical' heat-flow is below 70 mW/m², intersecting the solidus in intraplate locations at ~85 km and 1100 °C (for the MORB pyrolite composition). For further decrease in heat-flow to the 'steady-state' geotherm chosen as 50 mW/m², the solidus intersection remains at 80-90 km depth, even though the *dehydration solidus temperature* at this depth

1 drops to 1050 °C (Fig. 2). These depths and temperatures are typical for the LAB in oceanic or
2 young continental lithosphere, or MLDs in sub-cratonic lithosphere.

3
4 Our major argument is that lithospheric and asthenospheric mantle contain H₂O and
5 pargasite is a stable phase in lherzolitic upper mantle at low bulk water contents characteristic
6 for MORB mantle (~ 200 ppm) or higher water contents as in OIB or intraplate mantle
7 (depleted and refertilised). Thus the solidus of the shallow upper mantle is generally the
8 *pargasite dehydration solidus* to 90 km depth (~ 3 GPa) and *the vapour-saturated solidus for*
9 *lherzolite (+ C,H,O)* at greater depths. We have used a previously published model for the
10 thermal behaviour of stretched and thinned lithosphere, accompanied by adiabatic
11 asthenospheric upwelling (Royden and Keen 1980). In pressure (depth) and temperature
12 space, by overlaying the experimentally determined solidi for fertile and enriched model
13 mantle compositions on to the model for lithospheric thinning we predict a distinctive melting
14 pattern due to the role of pargasite in water storage and control of the solidus to ~90 km
15 depth. As previously argued this melting behaviour provides an explanation for the LAB and
16 the upper and lower boundaries of the LVZ. It is also important that the amount of melt
17 generated at the dehydration solidus is dependent on the subsolidus water content (modal
18 pargasite) (Green and Liebermann 1976; Green et al. 2014; Green 2015)
19
20
21
22
23
24
25
26
27
28
29
30

31 32 **Methodology**

33 34 35 36 *A possible empirical test of the applicability of the pargasite dehydration solidus*

37
38
39
40 The shape of the pargasite dehydration solidus (**Fig. 1**) has important implications for
41 predicting the onset of partial melting in the shallow upper mantle which may approximately
42 equate the position of the LAB or MLD:
43
44

45 1) The *pargasite lherzolite dehydration solidus* has roughly constant temperatures [~
46 1050 °C for more depleted compositions (Tinaquillo Lherzolite), and ~ 1100 °C for fertile
47 compositions (MOR Pyrolite, HZ lherzolite, Green 2015) in the depth interval between 1 GPa
48 (~ 30 km¹) and 2.8 GPa (~ 84 km; **Fig. 1**). The *pargasite lherzolite dehydration solidus*
49 temperature is slightly higher (~1150 °C) for enriched compositions (Hawaiian Pyrolite, NHD
50 peridotite; Wallace and Green 1991; Green 2015), however, we use the lower temperatures
51 (1050 and 1100 °C) corresponding to more depleted and fertile peridotite as it resembles more
52
53
54
55
56
57
58

59 ¹ for the calculation we generally assumed ~ 3 g/cm³ density for the lithosphere where 1 Kbar or 0.1 GPa
60 correspond to ~3 km thickness
61
62
63
64
65

1 closely the composition of the upper mantle beneath the CPR (see our following chapter on
2 xenoliths). This means that in this depth interval the presence of partial melt is expected if the
3 geotherm reaches the *dehydration solidus* temperatures. Geotherms in **Figure 2** specific for
4 the CPR (see how these were derived in following chapter) refer to the depth-temperature
5 curves for specific surface heat flow values whereas the 1050 °C and 1100 °C isotherms
6 approximate to the *dehydration solidi* between 1 – 2.8 GPa.
7
8
9

10 2) There is a sharp *negative* dT/dP in the dehydration solidi between 2.8 – 3 GPa (**Fig.**
11 **1**), with the solidus temperature *decreasing* by 50-100 °C with increasing pressure over a
12 depth interval of 5 - 6 km. (e.g. Green 1973; Niida and Green 1999; Green and Falloon 2005;
13 Green et al. 2014; Green 2015) This means that the depths of intersections of geotherms
14 calculated for heat flows of ~slightly below 70 mW/m² with the solidus for lherzolite with
15 ~200 ppm remain stable at ~85 - 90 km depth. Equally, for the early stages of a developing
16 continental rift, upwelling asthenosphere freezes to pargasite (± phlogopite) lherzolite at 85 -
17 90 km depth (**Fig. 1** and **2**) until the temperature at this depth exceeds the *pargasite*
18 *dehydration solidus temperatures*. If the uppermost part of the asthenosphere in intraplate
19 regions is fertile or depleted lherzolite then the LAB does not move to shallower depths
20 (thinning of lithosphere) until the heat flow exceeds ~70 mW/m². If the geotherm exceeds that
21 calculated for ~70 mW/m², then the intersection with the *dehydration solidus* moves rapidly
22 to shallower depths. This heat flow is the already defined *critical heat flow* which may be
23 different in other tectonic setting depending on the area specific depth-temperature curves.
24 The use of the *dehydration solidus* to map the depth to the LAB in an intraplate setting of
25 stretching and rising geotherms predicts an initial slow heating with no change to the
26 lithosphere thickness followed by a sharp change to more rapid rifting, rise of the LAB and
27 increasing intraplate magmatism.
28
29
30
31
32
33
34
35
36
37
38
39
40
41
42
43

44 In this paper we attempt to test the predictions of the *pargasite dehydration solidus* for
45 the LAB in the CPR using geophysical data. First it is assessed whether the depths of the 1050
46 and 1100 °C isotherms (approximating to the *dehydration solidi* at 1 - 2.8 GPa or ~30 – 85
47 km) in the Pannonian Basin (referred to PB hereafter) coincide with the location of the
48 geophysically constrained depth of the LAB. This is because the PB is a young continental rift
49 in the central CPR with highly attenuated lithosphere and high surface heat flow (> ~ 70
50 mW/m²) generally exceeding the *critical heat flow* where depth-temperature curves are
51 expected to cross the *pargasite dehydration solidus* depths less than 85-90 km (see preceding
52 discussion; **Fig. 1**). The PB is an excellent natural laboratory for such test as numerous
53 surface heat flow data, specific depth-temperature curves (geotherms), joint seismic and
54
55
56
57
58
59
60
61
62
63
64
65

1 magnetotelluric constraints on the depth of the LAB are available (Lenkey 1999; Lenkey et al.
2 2002; Horváth 1993; Tari et al. 1999; Horváth et al. 2006; 2015). Our approach is somewhat
3 simplified in the sense that the shape of the *dehydration solidus* is approximated by constant
4 (1050 and 1100 °C) temperatures between 1 and 3 GPa to simplify calculations. As the Moho
5 discontinuity is at ~25-30 km depth beneath the PB the small positive dT/dP at <1 GPa is not
6 considered. On the other hand, the strongly negative dT/dP at 2.8-3GPa effectively fixes the
7 LAB at 85 - 90 km as previously discussed. By ignoring any curvature in the solidus between
8 2.5 and 3 GPa our results may overestimate depth to the LAB only by a few km.
9
10
11
12
13
14
15

16 *Determination of temperature-depth curves and the depth of the 1050 and 1100 °C isotherms*
17
18 *for the PB*
19

20 The PB was formed by lithospheric extension during the Middle Miocene (Royden et al.
21 1983, Csontos et al. 1992; Horváth 1993) and this was accompanied by asthenospheric uplift
22 resulting in high surface heat flow (Dövényi and Horváth 1988; Lenkey et al. 2002). Since the
23 formation of the basin, the lithosphere has been cooling as evidenced by thermal subsidence
24 and accumulation of thick Neogene and Quaternary sediment pile (Magyar et al. 2012).
25 Therefore, steady state thermal models similar to those applied to the Fennoscandinavian
26 Shield (Artemieva 2009) or the Canadian Shield (Jaupart et al. 1998) cannot be applied to
27 estimate the geotherm in the lithosphere. We used the non-uniform stretching model of
28 Royden and Keen (1980), which takes into account the transient cooling of the lithosphere,
29 and allows the different amounts of stretching of the crust and lithospheric mantle.
30 Additionally, we took into account the radioactive heat production in the upper crust. The
31 inset in **Fig. 2** shows the initial geotherm before stretching and just after stretching. Following
32 the stretching the lithosphere cools and the temperature returns to its initial value which takes
33 about 100 million years. Given the stretching factors of the crust and the lithospheric mantle
34 the model predicts the evolution of the surface subsidence and heat flow.
35
36
37
38
39
40
41
42
43
44
45
46

47 The crustal and lithospheric mantle stretching factors for the model were derived in 5
48 x 5 km grid in the PB by equating the model-predicted present day heat flow and the total
49 accumulated sediment thickness with the observed values (Lenkey 1999). The thermal
50 parameters of the model are given in **Table 1**. It is evident that in case of higher heat flow the
51 stretching factors are also higher, and the geotherm in the lithosphere is steeper. We choose
52 four places near to the PGT-1 seismic section where the heat flow is 70, 80, 100 and 120
53 mW/m², respectively, and using the stretching factors previously derived (Lenkey 1999) and
54 belonging to these locations, the present day geotherms were calculated (thick lines in **Fig. 2**)
55
56
57
58
59
60
61
62
63
64
65

1 and the intersections of the geotherms with the pargasite dehydration solidus temperatures
2 (1050 and 1100 °C) were determined.

3
4 In their influential paper on the thermal behaviour of crustal stretching and
5 consequential mantle upwelling, McKenzie and Bickle (1988) divided the Earth's upper
6 mantle into underlying convecting layer, assumed to have an adiabatic temperature gradient,
7 overlain by a thermal boundary layer in which the gradient is steeper (super-adiabatic) from
8 surface temperatures to intersect the mantle adiabat at depths determined by local heat flow
9 and thermal conductivity. The term 'Mechanical Boundary Layer' (MBL) referred to the
10 uppermost mantle and crust with conductive heat transfer, overlying a transitional layer
11 ('Thermal Boundary Layer') (TBL), also with dT/dP greater than the adiabatic geothermal
12 gradient.
13
14
15
16
17
18
19

20 In our thermal model the bottom of the thermal lithosphere is at 120 km depth and
21 1300 °C based on the analysis of the ocean floor bathymetry (McKenzie 1978 after Parsons
22 and Sclater 1977). This depth and temperature for the base of the thermal lithosphere,
23 however, seems to be inconsistent with petrological models at the first sight (cf. Green, 2015).
24 This discrepancy arises from different uses of 'lithosphere' as we discussed above. The
25 geophysical model uses the thickness of the thermal lithosphere and not the petrological or
26 rheological lithosphere (e.g. Artemieva 2009). By definition from thermal point of view we
27 can distinguish the conductive, transitional and convective part of the upper mantle. The
28 conductive (MBL) part can be equated to the petrological lithosphere. The thermal
29 lithosphere, however is thicker and has a transitional thickness between the purely conductive
30 and convective upper mantle (TBL) (Artemieva 2009). It follows that the thermal lithosphere
31 includes the upper part of the asthenosphere as well. Consequently the 1300 °C at 120 km is
32 consistent with the petrological model, since 120 km is not the thickness of the petrological
33 lithosphere but that of the thermal lithosphere. The temperature at the top of the purely
34 convective asthenosphere is referred to as the potential temperature (T_p) and is assumed to be
35 ~1430 °C for the modern Earth (Green 2015). At the bottom of the thermal lithosphere the
36 temperature approaches T_p , which we assumed to be 1300 °C but its value is uncertain.
37 Uncertainty in this temperature is explored by varying its value from 1250 to 1450 °C.
38 Therefore, geotherms corresponding to heat flow of 50 to 120 mW/m² are calculated to
39 intersect a range of adiabatic gradients at a chosen depth of 120 km, and temperatures of 1250
40 °C to 1450 °C (i.e. corresponding to T_p ~1210 °C to 1410 °C). The geothermal model is quite
41 robust, because the depth to the intersections with 1050 and 1100 °C isotherms differ between
42 3 km (1250 °C) to 5 km (1450 °C) (**Fig. 2**). This means that the solidus/geotherm
43
44
45
46
47
48
49
50
51
52
53
54
55
56
57
58
59
60
61
62
63
64
65

1 intersections lie at slightly shallower depth if the assumed temperature at 120 km depth is
2 higher and vice versa. The inset **Fig. 2** illustrates a steady-state or pre-thinning geotherm for
3 50 mW/m² perturbed instantaneously by asthenospheric upwelling with T_p ~ 1300 °C.
4
5

6 7 **Results and Discussion**

8 9 10 *The depth of the 1050 and 1100 °C isotherms beneath the CPR and implications*

11
12
13
14 Using the geotherms calculated from the stretching model the local positions to the
15 *dehydration solidus* temperatures (1050 and 1100 °C) in the CPR were mapped (**Fig. 3a** and
16 **3b**). The maps reveal that the geotherm intersections with 1050 and 1100 °C isotherms are
17 shallower than 90 km in the PB which is characterized by heat flow values exceeding the
18 critical value (> ~ 70 mW/m²). The depth of both geotherm/solidus intersections decreases
19 very rapidly from below 90 km at the boundaries of the CPR to ~ 60 km in the inner part of
20 PB. This steepening of the geotherm happens usually over a short (~ 100 km) horizontal
21 distance. The depth of the geotherm/solidus intersections (approximated to 1050-1100 °C
22 isotherms) is ~60 km in large part of the central part of the CPR. There are some locations
23 (Transdanubian Central Range, Mecsek and Bükk Mts.), however, where the
24 geotherm/solidus intersections are in a deeper position. This deviation is due to the intensive
25 cooling effect of karst water circulation in the Mesozoic carbonate formations in these
26 regions. For the Transdanubian Central range the relatively lower heat flow can also be
27 related to the relatively thicker MOHO beneath the area (~30 – 35 km; Kiss et al. 2016)
28
29 The difference between the depths of the 1050 and 1100 °C geotherm/solidus intersections are
30 usually within ~ 6 km under the entire CPR. This is probably in the order of or less than the
31 uncertainty how accurately the depth of the isotherms could be constrained. This difference
32 could represent the apparent variation which arises from geochemistry of pargasite as in more
33 fertile (richer in Al, Ti, Fe and alkalis) mantle sources pargasite breaks down at 1150 °C,
34 while those from a more depleted source at only 1050 °C. This means that the pargasite break-
35 down in areas with more fertile upper mantle is expected to take place a few kilometers
36 deeper.
37
38
39
40
41
42
43
44
45
46
47
48
49
50
51
52
53
54

55 **Figure 4a** and **Figure 4b** display the difference in kilometers between the *dehydration*
56 *solidus* temperatures (1050 and 1100 °C) and the LAB determined by integrated
57 seismological observations and magnetotelluric soundings. For the overwhelming portion of
58
59
60
61
62
63
64
65

1 the PB the difference between the two independently determined LAB depth is much less than
2 ± 10 km. Consequently, we can state that these results at least do not disagree with the
3 prediction of our simple petrologic model based on the *dehydration solidus*. In fact, the
4 agreement between the position of the *dehydration solidus* temperatures and the geophysically
5 determined LAB is almost within model uncertainty ($\pm \sim 5$ km). This reasonable agreement
6 implies that in areas with similarly high heat flow to the PB (young rift areas and oceanic
7 plates) the position of the *dehydration solidus* (1050 and 1100 °C) may give good first order
8 estimation for the depth of the LAB.
9

10
11
12
13
14 Larger discrepancies exceeding 20 km in the PB are usually only observed for areas
15 where surface heat flow is underestimated (mountain ranges consists of carbonate formation,
16 see **Fig. 3**). At these areas the position of the *dehydration solidus* isotherms (1050 and 1100
17 °C) are deeper than the geophysically constrained LAB. The calculated *dehydration solidus*
18 isotherms also predict deeper LAB than the geophysically determined one in the central part
19 of the Great Hungarian Plain and in the Transylvanian basin (see **Fig. 4a** and **Fig. 4b**).
20
21
22
23
24

25
26 The particular part of the Great Hungarian Plain, where the calculated dehydration
27 solidus temperatures run deeper than the LAB, is characterized by extremely thinned
28 lithosphere, where the lithospheric thickness is only ~ 40 km in the Békés basin (at the SE
29 corner of this anomaly). This is also an area where deep basins (e.g. Makó basin and Békés
30 Basin) separated by elevated basement highs (e.g. Battonya high) with a NW-SE strike. These
31 deep basins were formed in the Late Miocene (~ 5 Ma, Early Pannonian; Horváth et al.,
32 2010), after the main phase of larger-scale extension in the CPR (Huisman et al. 2001) in the
33 Middle Miocene. This process may have been associated with the additional localized
34 thinning of the lithosphere which can account for the extremely thin lithosphere in this area.
35 Note that anomalous MOHO was identified in the Békés basin which may have been the
36 result of basaltic underplating in association with this relatively young regional rifting (Hajnal
37 et al. 1996). The relatively young rifting event here may imply that in this area the thermal
38 equilibrium might not yet have been completely achieved.
39
40
41
42
43
44
45
46
47
48

49 The Transylvanian Basin, on the other hand, is an elevated basin ($\sim 300 - 400$ m
50 above the sea level) between the Apuseni Mts. and East Carpathians, which is characterized
51 by thicker lithosphere and much lower surface heat flow than the PB. The discrepancy
52 between our prediction and the observed lithospheric thickness is related to the distinct
53 geodynamic history of Transylvanian Basin, because it was formed by different mechanisms
54 to the PB of which exact kinematics is yet to be revealed (e.g. Krézsek and Bally 2006).
55
56
57
58
59
60
61
62
63
64
65

Xenoliths

1
2
3
4 It is logical to evaluate whether equilibrium temperatures recorded by upper mantle xenoliths
5 from the central PB (Bakony-Balaton-highland) fit into our thermal approach. The studied
6 xenoliths from the PB span a considerable range of equilibrium temperatures from ~850 to
7 1175 °C (i.e. Embey-Isztin et al. 1989; 2001; Szabó et al. 2004; Dobosi et al. 2010; Kovács et
8 al. 2012; Embey-Isztin et al. 2014). The mantle xenoliths mainly originate from the
9 lithospheric mantle and only subordinately from the asthenosphere due to the less plastic
10 nature of the former. Thus, the maximum equilibrium temperatures (1175 ± 20 °C) seem to
11 only slightly exceed what we would expect if the LAB was related to the break-down of
12 pargasitic amphibole (i.e. max. 1150 °C in very fertile peridotite). This slight discrepancy
13 may be accounted for by the fact that xenoliths record older temperatures of the upper mantle
14 than those estimated from the present day surface heat flow. The age of the alkaline basaltic
15 activity which brought up the xenoliths to the surface is ~ 5 Ma. It means that there was time
16 for further thermal relaxation involving further subsidence of isotherms. During this process
17 the upper mantle which had originally 1175 °C equilibrium temperature at 5 Ma cooled
18 presumably below at least the *dehydration solidus* temperature (~1100 °C). The higher
19 temperatures of some upper mantle xenoliths may also reflect their asthenospheric origin. In
20 either case, the equilibrium temperatures of upper mantle xenoliths from the Bakony-Balaton
21 highland seem to be in line with our assumption that the LAB can be equated with the
22 *dehydration solidus* temperatures (1050 and 1100 °C) in a young rift area with high heat flow
23 values exceeding the *critical heat flow* ($> \sim 70$ mW/m²). In addition pargasitic amphibole can
24 be found either as a rock-forming mineral constituent or in traces in these upper mantle
25 xenoliths (i.e. Embey-Isztin 1974; Szabó et al. 2004; Dobosi et al. 2010).
26
27
28
29
30
31
32
33
34
35
36
37
38
39
40
41
42
43
44

Implications for the depth of the LAB beneath (young) oceanic plates

45
46
47
48
49 In summary, we can state that – albeit our estimation bears uncertainties ($\sim \pm 5$ km) – the
50 calculated and independently constrained depth of the LAB appears to agree reasonably well
51 (mostly within ± 5 km) beneath the PB. The PB is a young continental rift area where the
52 surface heat flow exceeds the *critical heat flow*. This is the particular heat flow value at which
53 the corresponding geotherm reaches the *dehydration solidus* temperatures (1050 and 1100 °C)
54 shallower than ~ 3 GPa (~ 85 - 90 km).
55
56
57
58
59
60
61
62
63
64
65

1 Below with a brief overview of the literature we explore whether the *dehydration*
2 *solidus* could predict the depth of the LAB under young oceanic plates where the heat flow is
3 usually above the critical value. Note that Green and Liebermann (1976) already put forward
4 that the top of the low velocity zone (i.e. LAB) under oceanic lithospheres is defined by the
5 intersection of the oceanic geotherm with the *dehydration solidus* of enriched or fertile
6 lherzolite from 0.5 to 2.8 GPa at ~1050-1100 °C. Because the geotherms become less steep
7 with increasing distance from the mid-ocean ridge, the lithosphere thickens with age and
8 distance from the middle ocean ridge. The steep negative dT/dP of the dehydration solidus at
9 2.8-3 GPa means that the lithosphere reaches a stable thickness of ~85-95 km for oceanic
10 plates older than 80 Ma. Thus it will be evaluated further whether this classic model and in
11 particular the position of the *dehydration solidus* could, indeed, coincide with the depth of the
12 LAB beneath young oceanic plates.
13
14
15
16
17
18
19
20

21 Rychert and Shearer (2011) studied the shape of stacked SS waveforms (SS
22 lithospheric profiling) in the Pacific Ocean and arrived to the conclusion that the depth of the
23 LAB beneath oceanic plates varies from 25 to 130 km and correlates with the distance from
24 the trench. They found that the depth of the detected geophysical anomalies agrees well with
25 the 930 ±90 °C isotherm(s) (95% of the data fall within this range) calculated from a half-
26 space cooling model with upper mantle potential temperature of 1350 °C and plate velocity of
27 60 mm/yr. The authors proposed that this boundary should be a permeability boundary with a
28 small amount of melt below it. Note that the proposed 930 ±90 °C is not very far from the
29 *dehydration solidus* temperatures, especially if we consider that the *dehydration solidus*
30 should be at lower temperatures (~ 1050 °C) in a depleted oceanic upper mantle. In addition
31 the authors used 1350 °C potential temperature which is ~ considerably lower than the
32 petrologically more reasonable 1430 °C (Green 2015). If the initial starting temperature in
33 their half-space cooling model was higher it is possible that the best fit isotherm would be
34 even closer to the *dehydration solidus* temperature.
35
36
37
38
39
40
41
42
43
44
45
46

47 Schmerr (2012) stacked a large dataset of SS precursors from oceanic areas and found
48 a sharp velocity contrast at 40-70 km depth. It was found that the depth of the discontinuity
49 show relatively good agreement with the depth of the 900 and 1100 °C isotherms predicted
50 from the half-space cooling model and the plate model respectively. The author attributed this
51 anomaly to the combination of the presence of small amounts of partial melts (0.1 - 3%) at the
52 base of the oceanic lithosphere, compositional contrast (i.e. depleted asthenosphere below a
53 re-hydrated more fertile lithosphere) and the cooling of the oceanic lithosphere with age.
54
55
56
57
58
59
60
61
62
63
64
65

1
2
3
4
5
6
7
8
9
10
11
12
13
14
15
16
17
18
19
20
21
22
23
24
25
26
27
28
29
30
31
32
33
34
35
36
37
38
39
40
41
42
43
44
45
46
47
48
49
50
51
52
53
54
55
56
57
58
59
60
61
62
63
64
65

Localized small-scale convections and hydrations enrichments (i.e. subductions) may further complicate this picture locally. Again the proposed temperature range overlaps with that of the *dehydration solidus* temperatures. The agreement may be even better if we consider that the author assumed again the same low upper mantle potential temperature as Rychert and Shearer (2011).

Naif et al. (2013) reported that there is presumably a melt rich layer beneath the oceanic plate subducting below Nicaragua based on electromagnetic soundings. The authors found that the high conductivity zone is between 45 and 70 km, of which upper part at 45 km could be defined as the LAB in our sense. This depth according to the authors is very close to the intersection of a 23 Ma old oceanic geotherm (corresponding to 1420 °C mantle potential temperature) and the solidus of peridotite containing 275±85 ppm ‘water’. Alternatively the intersection of an oceanic geotherm (corresponding to 1315 °C upper mantle potential temperature) and a peridotite solidus with 505±155 ppm water would be also at ~ 45 km. The MORB mantle, however, contains usually ‘only’ 50 - 200 ppm water which would be insufficient to produce partial melting. Naif et al. (2013) argued that this discrepancy may be explained by the uncertainties in the estimation of the solidus temperature and the presence of other volatiles. We suggest that the stability of pargasitic amphibole at low bulk water contents typical for MORB and the lower temperature of the *pargasite dehydration solidus* may more suitably explain this ‘discrepancy’. The *dehydration solidus* temperature (1050 and 1100 °C) would intersect their geotherm very close to the expected ~ 45 km depth.

In summary, it seems that the *pargasite dehydration solidus* and the classic petrological model of Green and Liebermann (1976) - while there are still some discrepancies - seem to give a reasonable explanation for the presence of a small amount of partial melts where geophysical anomalies likely indicating the LAB. It should be evaluated further, however, how other volatiles (especially CO₂) and the higher modal abundance of pargasite below the dehydration solidus would improve the correspondence between petrological and geophysical constraints on the depth of the LAB beneath oceanic basins.

Reconciling the relation of the LAB and MLD?

In the marginal areas of the CPR surrounding the PB, where the heat flow is below the *critical heat flow* for the area (< ~70 mW/m²) the discrepancy between the *dehydration solidus* temperatures and the geophysically determined LAB becomes large. This makes sense since the pargasitic amphibole breaks down at ~90 km depth uniformly in such areas. In these areas we expect to see a horizon of geophysical anomalies at ~ 90 km depth. These areas may

1
2
3
4
5
6
7
8
9
10
11
12
13
14
15
16
17
18
19
20
21
22
23
24
25
26
27
28
29
30
31
32
33
34
35
36
37
38
39
40
41
42
43
44
45
46
47
48
49
50
51
52
53
54
55
56
57
58
59
60
61
62
63
64
65

include older (Phanerozoic) continental and oceanic plates and cratons where surface heat flow is below the *critical heat flow*.

In **Figure 5** it is illustrated how the relation of the LAB and MLD may vary in 1) young continental rifts and oceanic plates, 2) Phanerozoic continental lithospheres and older oceanic plates and 3) cratons. The main point is that in young continental rifts and oceanic basins the identification of the LAB is usually straightforward. In these areas the LAB is mainly related to the break-down of pargasite at the *dehydration solidus* temperatures (1050 and 1100 °C isotherms).

In contrast in older Phanerozoic continental lithospheres, older oceanic plates or cratons where the heat flow is below the *critical value* the pargasite breaks down at ~ 90 km, which should cause geophysical anomalies at a relatively constant depth globally. Indeed. Thybo and Perchuc (1997) and Thybo (2006) were among the first to reveal the presence of a global layer of geophysical anomalies at ~100 km, referred to as the 8° discontinuity. Its origin, have been explained by several possible scenarios including the presence of partial melt but no significance was attached to the role of pargasitic amphibole. Kind et al. (2012) reported that the top of the low velocity zone (LVZ) is sharper and appears to be a global horizon (at depth ~100 km). This anomaly seems to be present below cratonic areas as well. Their study was based on receiver function analysis of a global dataset of converted S and P phases. Kind et al. (2012) argued that the global anomaly may be related to the role of aluminous orthopyroxene (Mierdel et al. 2007) or EAGBS (Karato 2014). Fischer et al. (2010) also reported a global layer at ~100 km (including oceans and cratons) which is perturbed by upwelling (plumes) and down welling (subductions) in the mantle. This boundary is characterized by steep velocity gradients reflected in ScS reverberations and P and S receiver function analysis. They argued that its origin is not only related to the thermal gradient but hydration, presence of melt and anisotropy may all play a role. The ~100 km depth of global geophysical anomalies agrees very well with the upper stability (~ 90 km) of pargasite in areas where heat flow is low. Thus, it appears to be reasonable to attribute the origin of this global boundary layer dehydration solidus of the pargasite bearing upper mantle at low bulk water contents.

Consequently in Phanerozoic continental lithospheres and older oceanic plates the geophysical anomalies generated by the pargasite melting at 90 km may not always be clearly distinguished from those of the sometimes only slightly deeper LAB (**Fig. 5**) We argue that in many previous studies the shallower anomalies interpreted as the MLD may be produced by the melting of pargasite at ~ 90 km (i.e., Abt et al. 2010; Selway et al. 2015). In cratonic areas

1 where the LAB is very deep (> 150 km) the anomaly caused by the pargasite dehydration can
2 easily be discerned from the LAB by the much shallower depth of the former (**Fig. 5**). This is
3 not to say that all MLDs can be explained in Phanerozoic continental lithospheres, older
4 oceanic plates and cratons by the pargasite melting at ~ 90 km. What we want to stress here is
5 that some MLDs detected in these areas could be related to pargasite dehydration as argued by
6 Selway et al. (2015).
7
8
9

10 Note that there are similar anomalies present at ~ 100 km depth in other continental
11 areas with thicker lithosphere as well (e.g. North America, Abt et al. 2010) which are also
12 interpreted as MLDs. Rader et al. (2015) argued that the MLD is the geophysical
13 manifestation of a geochemical boundary which may be due to the prior intersection of the
14 volatile-rich solidus with cooling geotherms. They also suggested that the MLD marks the
15 former position of the LAB when the lithosphere was tectonically younger and presumably
16 warmer. Rader et al. (2015) implied the presence of higher modal abundance of phlogopite,
17 carbonate or pyroxene may account for the slower seismic waves at the MLD but attributed
18 only moderate roll to the pargasite *dehydration solidus*. In their study the average of accurate
19 geophysical MLD determinations was 92 km with the vast majority of the data vary between
20 80 and 110 km. This agrees very well with pargasite melting at ~ 3 GPa (90 km).
21
22
23
24
25
26
27
28
29
30

31 In Hansen et al. (2015) the depth of the MLD and LAB was estimated based on S_p
32 receiver function imaging focusing on the position of negative velocity gradients (NVG). The
33 authors proposed that NVGs in the western US indicates the LAB which is at 60-85 km with
34 temperatures between 1200-1400 °C. In contrast, the NVGs under the central US and Rockies
35 are between 70 and 110 km at temperatures 700-900 °C. These are mainly interpreted as
36 MLDs but there is an area between the Rockies and the central US where the interpretation of
37 NVGs is ambiguous (they could indicate both LAB and MLD). The temperatures were
38 estimated from surface wave tomography model originating from the USArray dispersion
39 measurements using the olivine inelasticity model of Faul and Jackson (2010) assuming an
40 average grain size of 1 mm for upper mantle rocks. The model, however, is strongly grain size
41 dependent and larger average grain size could result in higher temperatures. Considering
42 normal intra-plate geotherms (**Fig. 2**) the MLD temperatures seems to be unusually low while
43 LAB temperatures exceptionally high from petrological point of view. Thus, our preferred
44 interpretation is that in the western US the heat flow should be above the critical value and the
45 pargasite dehydration solidus temperatures are reached shallower than ~ 90 km. Consequently
46 NVGs under the western US indicate indeed the LAB, however, the corresponding
47 temperatures at that depth should not exceed ~ 1100 °C (which is much lower what the authors
48
49
50
51
52
53
54
55
56
57
58
59
60
61
62
63
64
65

1
2
3
4
5
6
7
8
9
10
11
12
13
14
15
16
17
18
19
20
21
22
23
24
25
26
27
28
29
30
31
32
33
34
35
36
37
38
39
40
41
42
43
44
45
46
47
48
49
50
51
52
53
54
55
56
57
58
59
60
61
62
63
64
65

claimed). In the other areas on the east the heat flow should be below the critical value and pargasite melts at ~ 90 km. In our interpretation, the transitional area between the western and central US, where the assignment of the NVGs is ambiguous, represents a situation where it cannot be accurately predicted whether the pargasite break-down at ~90 km could correspond to the LAB or MLDs. Further to the east under the central US the LAB is deeper and can be well resolved from the pargasite break down at ~90 km. This depth seems to be in line with the 84 km peak in NVGs' depth under the central US. The calculated temperature (~770 °C) for the MLD, however, appears to be underestimated.

Selway et al. (2015) suggested that MLD phase could be commonly explained by the stability of (pargasitic) amphibole, however, the amphibole alone may not be the universal explanation. The authors argue that in some localities (e.g. Kaapval craton) where the MLD is well constrained and upper mantle xenoliths are available the amphibole is not present in sufficient modal abundance from MLD depths to account for the observed decrease in seismic velocities. Selway et al. (2015) considered only the effect of modal amphibole on seismic velocities but did not take into account the role of small amount of melts/fluids which should exist at the pargasite *dehydration solidus*. It may well be that the combined affect of (very) small amount of modal pargasite and underlying incipient melt bearing upper mantle mineralogy may give better fit to their observations. We certainly agree of course that the stability of (pargasitic) amphibole is not the only factor in controlling the formation of geophysical anomalies in the upper mantle, therefore, 'discrepancies' may be reconciled with the consideration of these other factors (e.g. EAGBS, hydrolytic weakening).

Conclusions

A simple petrologic model based on the pargasite *dehydration solidus* in the shallow upper mantle has been tested whether it is suitable to explain the presence of geophysical anomalies at LAB and MLD depths. In young continental rifts and oceanic plates where the heat flow is above a critical value the model suggests that the position of the pargasite *dehydration solidus* temperatures in the upper mantle (1050 and 1100 °C isotherms) should agree well with the geophysically constrained LAB. In this study we demonstrated that in the *Pannonian Basin*, which is a young rift area, the depth of these isotherms indeed resemble well with the independently determined depth of the LAB. The critical surface heat flow is the heat flow value at which the area specific depth-temperature curves reaches the *dehydration solidus* temperatures in shallower depth than 3 GPa (~ 90 km). This ~ 90 km is the depth at which

pargasite ultimately breaks down if the *dehydration solidus* temperatures are not exceeded. This means that in areas where the surface heat flow below the *critical value* (older continental areas, oceanic plates and cratons) there should be a globally occurring horizon of geophysical anomalies at ~90 km. This appears to be in line with global geophysical observations. In Phanerozoic continental areas and oceanic slabs MLD occurring at ~90 km depth may be explained by the break-down of pargasitic amphibole. In these areas sometimes it may be difficult to distinguish the LAB from the MLD. In cratonic areas, however, the distinction between the LAB and MLD is more straightforward, and the latter could be due to the break-down of pargasitic amphibole at ~90 km.

1
2
3
4
5
6
7
8
9
10
11
12
13
14
15
16
17
18
19
20
21
22
23
24
25
26
27
28
29
30
31
32
33
34
35
36
37
38
39
40
41
42
43
44
45
46
47
48
49
50
51
52
53
54
55
56
57
58
59
60
61
62
63
64
65

Figure and Table captions

1
2
3
4 **Fig. 1.** The positions of the i) ‘Water-saturated’ (bulk H₂O ≥ 0.4 wt.%); ii) ‘*Dehydration*’ (0.4
5 wt.% ≥ bulk H₂O ≥ 190 wt.% ppm) and iii) ‘Anhydrous’ solidus (190 wt.% ppm ≥ bulk H₂O)
6 of upper mantle lherzolite in the P-T space. The Figure is modified after Fig. 3. in Green
7 (2015). Calculated solidus temperatures for various bulk water contents in ppm after Katz et
8 al. (2003) are also highlighted. The position of an ‘Intra-plate’ geotherm was also plotted for a
9 comparison. Different *dehydration solidi* temperatures correspond to upper mantle
10 compositions with different fertility. It is ~ 1050, 1100 and 1150 °C for refractory (Tinaquillo
11 lherzolite), fertile (MORB source mantle) and enriched (Hawaiian pyrolite) upper mantle
12 (Wallace and Green, 1991).
13
14
15
16
17
18
19
20
21

22 **Fig. 2.** Geotherms calculated from a non-uniform stretching model (Lenkey 1999 using the
23 model of Royden and Keen 1980), except curve 50, which is a steady-state geotherm. The
24 labels in the curves refer to observed heat flow values (in mW/m²) in the CPR near to seismic
25 section PGT-1. Thick curves are calculated with the usual boundary condition of 1300 °C at
26 120 km depth (McKenzie 1978; Royden and Keen 1980). Inlet: initial geotherm before
27 stretching and the geotherm just after stretching. Geotherms calculated based on different
28 assumed temperatures (1250, 1350, 1400 and 1450 °C) at 120 km are also indicated (see text
29 for more details). The position of the *dehydration* and *anhydrous* solidi for different bulk
30 upper mantle compositions are also indicated. Dense dotted lines indicate the position of the
31 *dehydration solidi* for TLZ, MPY and HPY upper mantle compositions, whereas less dense
32 dotted lines shows the position of the *anhydrous* solidi for MPY, HPY and Katz et al (2003)
33 as well. The least dotted lines represent the adiabats for mantle potential temperatures for
34 1280 and 1430 °C.
35
36
37
38
39
40
41
42
43
44
45
46

47 **Fig. 3. a)** Schematic geological map of the Carpathian Pannonian region (CPR). Major
48 localities are discussed in the text are indicated. Calculated depths of the *dehydration solidus*
49 isotherms of 1050 °C (**b**) and 1100 °C (**c**) are highlighted beneath the CPR using surface heat
50 flow data of Lenkey et al. (2002) and depth-temperature curves in **Fig. 2**. The location of the
51 PGT-1 geophysical traverse is indicated by solid line.
52
53
54
55
56
57

58 **Fig. 4.** Difference between the depths of the *dehydration solidus* temperatures 1050 °C (**a**)
59 and 1100 °C (**b**) and the geophysically constrained LAB (Tari et al. 1999) in kilometers.
60
61
62
63
64
65

1 **Fig. 5.** Variations in the respective positions of the lithosphere-asthenosphere boundary
2 (LAB) and middle lithospheric discontinuities (MLDs) in different tectonic settings. This
3 Ffigure is substantially modified and completed after **Fig. 1** in Fischer et al. (2010).
4
5
6
7

8
9 **Table 1.** Parameters applied for the calculation of depth temperature curves.
10

11 **References**

12
13
14
15
16 Abt DL, Fischer KM, French SW, Ford HA, Yuan H, Romanowicz B (2010) North American
17 lithospheric discontinuity structure imaged by Ps and Sp receiver functions. *Journal of*
18 *Geophysical Research: Solid Earth*, 115(B9). DOI: 10.1029/2009JB006914
19

20
21 Artemieva IM (2009) The continental lithosphere: reconciling thermal, seismic, and
22 petrologic data. *Lithos* 109(1):23-46.
23

24
25 Asimow PD, Dixon JE, Langmuir CH (2004) A hydrous melting and fractionation model for
26 mid-ocean ridge basalts: Application to the Mid-Atlantic Ridge near the Azores.
27 *Geochemistry, Geophysics, Geosystems*, 5(1). 2003GC000568. ISSN 1525-2027
28

29
30 Bell DR, Rossman GR (1992) Water in Earth's mantle: the role of nominally anhydrous
31 minerals. *Science* 255(5050): 1391.
32

33
34 Csontos L, Nagymarosy A, Horváth F, Kovác M (1992) Tertiary evolution of the Intra-
35 Carpathian area: a model. *Tectonophysics* 208:221-241
36

37
38 Danyushevsky LV, Eggins SM, Fallon TJ, Christie DM (2000) H₂O abundance in depleted to
39 moderately enriched mid-ocean ridge magmas; part I: incompatible behaviour, implications
40 for mantle storage, and origin of regional variations. *Journal of Petrology* 41(8):1329-1364.
41

42
43 Demouchy S, Bolfan-Casanova N (2016) Distribution and transport of hydrogen in the
44 lithospheric mantle: A review. *Lithos* 240:402-425.
45

46
47 Dietz RS (1961) Continent and Ocean Basin Evolution by Spreading of the Sea Floor. *Nature*
48 190(4779):854–857.

49
50 Dixon JE, Leist L, Langmuir C, Schilling JG (2002) Recycled dehydrated lithosphere
51 observed in plume-influenced mid-ocean-ridge basalt. *Nature*, 420(6914), 385-389.
52

53
54 Dobosi G, Jenner G, Embey-Isztin A, Downes H (2010) Cryptic metasomatism in clino- and
55 orthopyroxene in the upper mantle beneath the Pannonian region. In: Coltorti M (ed)
56 *Petrological evolution of the European lithospheric mantle: from Archaean to present day.*
57 *Geol Soc, London*, p 337
58
59
60
61
62
63
64
65

1 Dövényi P, Horváth F (1988) Heat flow map of the Pannonian basin and surrounding regions.
2 In: L.H. Royden and F. Horváth (Editors), *The Pannonian Basin, a Study in Basin Evolution*.
3 Amer. Assoc. Petr. Geol. Mem. p 45

4 Embey-Isztin A, Dobosi G, Altherr R, Meyer HP (2001) Thermal evolution of the lithosphere
5 beneath the western Pannonian Basin: evidence from deep-seated xenoliths. *Tectonophysics*
6 331:283–305.

7
8
9 Embey-Isztin A, Scharbert HG, Dietrich H, Poultidis H (1989) Petrology and geochemistry of
10 peridotite xenoliths in alkali basalts from the Transdanubian Volcanic Region, West Hungary.
11 *Journal of Petrology* 30:79–105.

12
13 Embey-Isztin A (1976) Amphibolite/lherzolite composite xenolith from Szigliget, North of
14 the Lake Balaton, Hungary. *Earth and Planetary Science Letters* 31:297–304.

15
16
17 Embey-Isztin A, Dobosi G, Bodinier JL, Bosch D, Jenner GA, Pourtales S, Bruguier O (2014)
18 Origin and significance of poikilitic and mosaic peridotite xenoliths in the western Pannonian
19 Basin: geochemical and petrological evidences. *Contributions to Mineralogy and Petrology*
20 168(3):1-16.

21
22
23 Falus G, Szabó C, Vaselli O (2000) Mantle upwelling within the Pannonian Basin: evidence
24 from xenolith lithology and mineral chemistry. *Terra Nova* 12(6):295-302.

25
26
27 Falus G, Szabó C, Kovács I, Zajacz Z, Halter W (2007) Symplectite in spinel lherzolite
28 xenoliths from the Little Hungarian Plain, Western Hungary: a key for understanding the
29 complex history of the upper mantle of the Pannonian Basin. *Lithos* 94(1):230-247.

30
31
32 Faul UH, Jackson I (2005) The seismological signature of temperature and grain size
33 variations in the upper mantle. *Earth and Planetary Science Letters* 234(1):119-134.

34
35
36 Fischer M, Ford H, Abt D, Rychert C (2010) The Lithosphere-Asthenosphere Boundary.
37 *Annual Review of Earth and Planetary Sciences* 38:551–575. doi:10.1146/annurev-earth-
38 040809-152438

39
40
41 Girard J, Chen J, Raterron P, Holyoke CW (2013) Hydrolytic weakening of olivine at mantle
42 pressure: Evidence of [100](010) slip system softening from single-crystal deformation
43 experiments. *Physics of the Earth and Planetary Interiors* 216:12-20.

44
45
46 Green DH (1971) Composition of basaltic magmas as indicators of conditions of origin:
47 application to oceanic volcanism. *Philos Trans R Soc Lond* 268:707–725.

48
49
50 Green DH (1973) Experimental melting studies on a model upper mantle composition at high
51 pressures under water-saturated and water-undersaturated conditions. *Earth Planet Sci Lett*
52 19:37–53.

53
54
55 Green DH, Liebermann RC (1976) Phase equilibria and elastic properties of a pyrolite model
56 for the oceanic upper mantle. *Tectonophysics* 32:61–92

57
58
59 Green DH (2015) Experimental petrology of peridotites, including effects of water and carbon
60 on melting in the Earth's upper mantle. *Physics and Chemistry of Minerals* 42(2):95-122.

61
62
63
64
65

1 Green DH, Hibberson WO, Kovács I, Rosenthal A (2010) Water and its influence on the
2 lithosphere-asthenosphere boundary. *Nature* 467(7314):448-451.
3

4 Green DH, Hibberson WO, Rosenthal A, Kovács I, Yaxley GM, Falloon TJ, Brink F (2014)
5 Experimental study of the influence of water on melting and phase assemblages in the upper
6 mantle. *Journal of Petrology* 55(10):2067-2096.
7
8

9 Griffin WL, Wass SY, Hollis JD (1984) Ultramafic xenoliths from Bullenmerri and Gnotuk
10 maars, Victoria, Australia: petrology of a sub-continental crust-mantle transition. *Journal of*
11 *Petrology* 25(1):53-87.
12
13

14 Hajnal Z, Reilkoff B, Posgay K, Hegedus E, Takacs E, Asudeh I, Ansorge J, DeIaco R (1996)
15 Crustal-scale extension in the central Pannonian basin. *Tectonophysics* 264(1):191-204.
16
17

18 Hammond WC, Humphreys ED (2000) Upper mantle seismic wave attenuation: Effects of
19 realistic partial melt distribution. *Journal of Geophysical Research: Solid Earth*, 105(B5):
20 10987-10999.
21
22

23 Hansen SM, Dueker K, Schmandt B (2015) Thermal classification of lithospheric
24 discontinuities beneath USArray. *Earth and Planetary Science Letters* 431:36-47.
25
26

27 Hauri E, Wang J, Dixon JE, King PL, Mandeville C, Newman S (2002) SIMS analysis of
28 volatiles in silicate glasses: 1. Calibration, matrix effects and comparisons with FTIR.
29 *Chemical Geology* 183(1):99-114.
30
31

32 Hirschmann MM (2010) Partial melt in the oceanic low velocity zone. *Physics of the Earth*
33 *and Planetary Interiors* 179(1):60-71.
34
35

36 Hirth G, Kohlstedt DL (1996) Water in the oceanic upper mantle: implications for rheology,
37 melt extraction and the evolution of the lithosphere. *Earth and Planetary Science Letters*
38 144(1):93-108.
39
40

41 Horváth F (1993) Towards a mechanical model for the formation of the Pannonian basin.
42 *Tectonophysics* 226(1):333-357.
43
44

45 Horváth F, Musitz B, Balázs A, Végh A, Uhrin A, Nádor A, Koroknai B, Pap N, Tóth T,
46 Wórum G (2015) Evolution of the Pannonian basin and its geothermal resources. *Geothermics*
47 53:328-352.
48
49

50 Horváth F, Bada G, Szafián P, Tari G, Ádám A, Cloetingh S (2006) Formation and
51 deformation of the Pannonian Basin: constraints from observational data. *Geological Society,*
52 *London, Memoirs* 32(1):191-206.
53
54

55 Huismans RS, Podladchikov YY, Cloetingh S (2001) Dynamic modeling of the transition
56 from passive to active rifting, application to the Pannonian basin. *Tectonics* 20(6):1021-1039.
57
58

59 Jackson I, Faul U, Skelton R (2014) Elastically accommodated grain-boundary sliding: New
60 insights from experiment and modeling. *Physics of the Earth and Planetary Interiors* 228:203-
61 210.
62
63
64
65

1 Jackson I, Faul UH (2010) Grainsize-sensitive viscoelastic relaxation in olivine: to-wards a
2 robust laboratory-based model for seismological application. *Phys. Earth Planet. Inter.*
3 (183):151–163.
4

5
6 Jaupart C, Mareschal JC (1999) The thermal structure and thickness of continental roots.
7 *Lithos* 48:93-114.
8

9
10 Jaupart C, Mareschal JC, Guillou-Frottier L, Davaille A (1998) Heat Flow and thickness of
11 the lithosphere in the canadian Shield. *J.Geoph. Res.*103(B7):15269-15286.
12

13 Karato SI (2014) Does partial melting explain geophysical anomalies? *Physics of the Earth*
14 *and Planetary Interiors* 228:300-306.
15

16
17 Karato SI, Olugboji T, Park J (2015). Mechanisms and geologic significance of the mid-
18 lithosphere discontinuity in the continents. *Nature Geoscience* 8(7):509-514.
19

20
21 Katz RF, Spiegelman M, Langmuir CH (2003) A new parameterization of hydrous mantle
22 melting. *Geochemistry, Geophysics, Geosystems* 4(9). DOI: 10.1029/2002GC000433
23

24
25 Kawakatsu H, Kumar P, Takei Y, Shinohara M, Kanazawa T, Araki E, Suyehiro K. (2009)
26 Seismic evidence for sharp lithosphere-asthenosphere boundaries of oceanic plates. *Science*
27 324(5926):499-502.
28

29
30 Kind R, Yuan X, Kumar P (2012) Seismic receiver functions and the lithosphere–
31 asthenosphere boundary. *Tectonophysics* 536:25-43.
32

33
34 Kiss J, Gúthy T, Zilahi-Sebes L (2016) A Mohorovičić-határfelület magyarországi kutatása–
35 módszerek, mérések, eredmények/Research of the Mohorovičić discontinuity in Hungary
36 (methods, measurements and results). *Magyar Geofizika* 56(3):152-178.
37

38
39 Kohlstedt DL, Keppler H, Rubie DC (1996) Solubility of water in the α , β and γ phases of
40 (Mg, Fe) 2SiO_4 . *Contributions to Mineralogy and Petrology* 123(4):345-357.
41

42
43 Konzett J, Armstrong RA, Günther D (2000) Modal metasomatism in the Kaapvaal craton
44 lithosphere: constraints on timing and genesis from U–Pb zircon dating of metasomatized
45 peridotites and MARID-type xenoliths. *Contributions to Mineralogy and Petrology* 139(6):
46 704-719.
47

48
49 Kovács I, Falus Gy, Stuart G, Hidas K, Szabó Cs, Flower MFJ, Hegedűs E, Posgay K, Zilahi-
50 Sebes L (2012) Seismic anisotropy and deformation pat-terns in upper mantle xenoliths from
51 the central Carpathian–Pannonian region: Asthenospheric flow as a driving force for Cenozoic
52 extension and extrusion? *Tectonophysics* 514–517:168–179.
53

54
55 Kovács I, Green DH, Rosenthal A, Hermann J, O'Neill HStC, HibbersonWO, Udvardi B
56 (2012) An experimental study of water in nominally anhydrous minerals in the upper mantle
57 near the water-saturated solidus. *Journal of Petrology* 53 (10):2067-2093.
58
59
60
61
62
63
64
65

1 Krézsek C, Bally W (2006) The Transylvanian Basin (Romania) and its relation to the
2 Carpathian fold and thrust belt: insights in gravitational salt tectonics. *Mar. Petrol. Geol.*
3 23:405–442. doi:10.1016/j.marpetgeo.2006.03.003.

4 Lambert IB, Wyllie PJ (1970) Low-velocity zone of the Earth's mantle: incipient melting
5 caused by water. *Science* 169(3947):764-766.

6
7
8 Lenkey L (1999) Geothermics of the Pannonian basin and its bearing on the tectonics of basin
9 evolution. PhD thesis, Vrije Universiteit, Amsterdam, 215 pp.

10
11
12 Lenkey L, Dövényi P, Horváth F, Cloetingh S (2002) Geothermics of the Pannonian basin and
13 its bearing on the neotectonics. In: Cloetingh S, Horváth F, Bada G and Lankreijer A. (Eds):
14 Neotectonics and surface processes: the Pannonian basin and Alpine/Carpathian system,
15 European Geosciences Union, Stephan Mueller Special Publication Series 3:29-40.

16
17
18 Magyar I, Radivojevic D, Sztanó O, Synak R, Ujszászi K, Pócsik M (2012) Progradation of
19 the paleo-Danube shelf margin across the Pannonian Basin during the Late Miocene and Early
20 Pliocene. *Global and Planetary Change* 103:168-173.

21
22
23 Mason RG, Raff AD (1961) Magnetic survey off the west coast of the United States between
24 32°N latitude and 42°N latitude. *Bulletin of the Geological Society of America* 72(8):1259–
25 1266.

26
27
28 McKenzie D (1978) Some remarks on the development of sedimentary basins. *Earth and*
29 *Planet. Sci. Lett.* 40:25-32

30
31
32 McKenzie D, Bickle MJ (1988) The volume and composition of melt generated by extension
33 of the lithosphere. *Journal of Petrology* 29:625-697.

34
35
36 Michael PJ (1988). The concentration, behavior and storage of H₂O in the suboceanic upper
37 mantle: Implications for mantle metasomatism. *Geochimica et Cosmochimica Acta*
38 52(2):555-566.

39
40
41 Mierdel K, Keppler H, Smyth JR, Falko L (2007) Water solubility in aluminous
42 orthopyroxene and the origin of Earth's asthenosphere. *Science* 315:364–368.
43 doi:10.1126/science.1135422.

44
45
46 Naif S, Key K, Constable S, Evans RL (2013) Melt-rich channel observed at the lithosphere-
47 asthenosphere boundary. *Nature* 495(7441):356-359.

48
49
50 Ni H, Keppler H, Behrens H (2011) Electrical conductivity of hydrous basaltic melts:
51 implications for partial melting in the upper mantle. *Contributions to Mineralogy and*
52 *Petrology* 162(3):637-650.

53
54
55 Niida K, Green, DH (1999) Stability and chemical composition of pargasitic amphibole in
56 MORB pyrolite under upper mantle conditions. *Contributions to Mineralogy and Petrology*
57 135(1):18-40.

1 Peslier AH (2010) A review of water contents of nominally anhydrous natural minerals in the
2 mantles of Earth, Mars and the Moon. *Journal of Volcanology and Geothermal Research*
3 197(1):239-258.

4 Posgay K, Bodoky T, Hegedüs E, Kovácsvölgyi S, Lenkey L, Szafián P, Varga G (1995)
5 Asthenospheric structure beneath a Neogene basin in southeast Hungary. *Tectonophysics*
6 252(1):467-484.

7 Rader E, Emry E, Schmerr N, Frost D, Cheng C, Menard J, Geist D (2015) Characterization
8 and Petrological Constraints of the Midlithospheric Discontinuity. *Geochemistry, Geophysics,*
9 *Geosystems*, 16(10):3484-3504.

10 Royden L, Keen CE (1980) Rifting process and thermal evolution of the continental margin of
11 Eastern Canada determined from subsidence curves. *Earth and Planet. Sci. Let.* 51:343-361.

12 Royden LH, Horváth F, Nagymarosy A, Stegena L (1983) Evolution of the Pannonian basin
13 system: 2. Subsidence and thermal history. *Tectonics* 2:91-137.

14 Rychert CA, Shearer PM (2011) Imaging the lithosphere-asthenosphere boundary beneath the
15 Pacific using SS waveform modeling. *Journal of Geophysical Research: Solid Earth* 116(B7)
16 DOI: 10.1029/2010JB008070

17 Carey SW (1958) The tectonic approach to continental drift. In: Carey SW (ed.): *Continental*
18 *Drift – A Symposium*. University of Tasmania, Hobart, 177-363 (expanding Earth from p.
19 311 to p. 349)

20 Saal AE, Hauri EH, Langmuir CH, Perfit MR (2002) Vapour undersaturation in primitive
21 mid-ocean-ridge basalt and the volatile content of Earth's upper mantle. *Nature* 419(6906):
22 451-455.

23 Schmerr N (2012) The Gutenberg discontinuity: Melt at the lithosphere-asthenosphere
24 boundary. *Science* 335(6075):1480-1483.

25 Selway K, Ford H, Kelemen P (2015) The seismic mid-lithosphere discontinuity. *Earth and*
26 *Planetary Science Letters* 414:45-57.

27 Smyth J, Bell DR, Rossman GR (1991) Incorporation of hydroxyl in upper-mantle
28 clinopyroxenes. *Nature* 351(6329):732-735.

29 Szabó C, Falus G, Zajacz Z, Kovács I, Bali E (2004) Composition and evolution of
30 lithosphere beneath the Carpathian–Pannonian Region: a review. *Tectonophysics* 393(1):119-
31 137.

32 Takei Y, Holtzman BK (2009) Viscous constitutive relations of solid-liquid composites in
33 terms of grain boundary contiguity: 1. Grain boundary diffusion control model. *Journal of*
34 *Geophysical Research: Solid Earth*, 114(B6). DOI: 10.1029/2008JB005850

35 Tari G, Dövényi P, Dunkl I, Horváth F, Lenkey L, Stefanescu M, Tóth T (1999) Lithospheric
36 structure of the Pannonian basin derived from seismic, gravity and geothermal data.
37 *Geological Society, London, Special Publications* 156(1):215-250.

1 Thybo H (2006) The heterogeneous upper mantle low velocity zone. *Tectonophysics* 416 (1–
2):53–79.
3

4 Thybo H, Perchuc E (1997) The seismic 8 degrees discontinuity and partial melting in
5 continental mantle. *Science* 275(5306):1626–1629.
6

7
8 Wallace M, Green DH (1991) The effect of bulk rock composition on the stability of
9 amphibole in the upper mantle: implications for solidus positions and mantle metasomatism.
10 *Mineralogy and Petrology* 44(1-2):1-19.
11

12
13 Warren JM, Hauri EH (2014) Pyroxenes as tracers of mantle water variations. *Journal of*
14 *Geophysical Research: Solid Earth* 119(3):1851-1881.
15

16
17 Wegener A (1912). "Die Entstehung der Kontinente". *Geologische Rundschau* (in German) 3
18 (4): 276–292. doi:10.1007/BF02202896.
19

20
21 Wilson JT (1963) Hypothesis on the Earth's behaviour. *Nature* 198(4884):849–865.
22

23 Xu Z, Gong B, Zhao Z (2016) The water content and hydrogen isotope composition of
24 continental lithospheric mantle and mantle-derived mafic igneous rocks in eastern China.
25 *Science China Earth Sciences* 59(5):910-926.
26
27
28
29
30
31
32
33
34
35
36
37
38
39
40
41
42
43
44
45
46
47
48
49
50
51
52
53
54
55
56
57
58
59
60
61
62
63
64
65

Figure 1

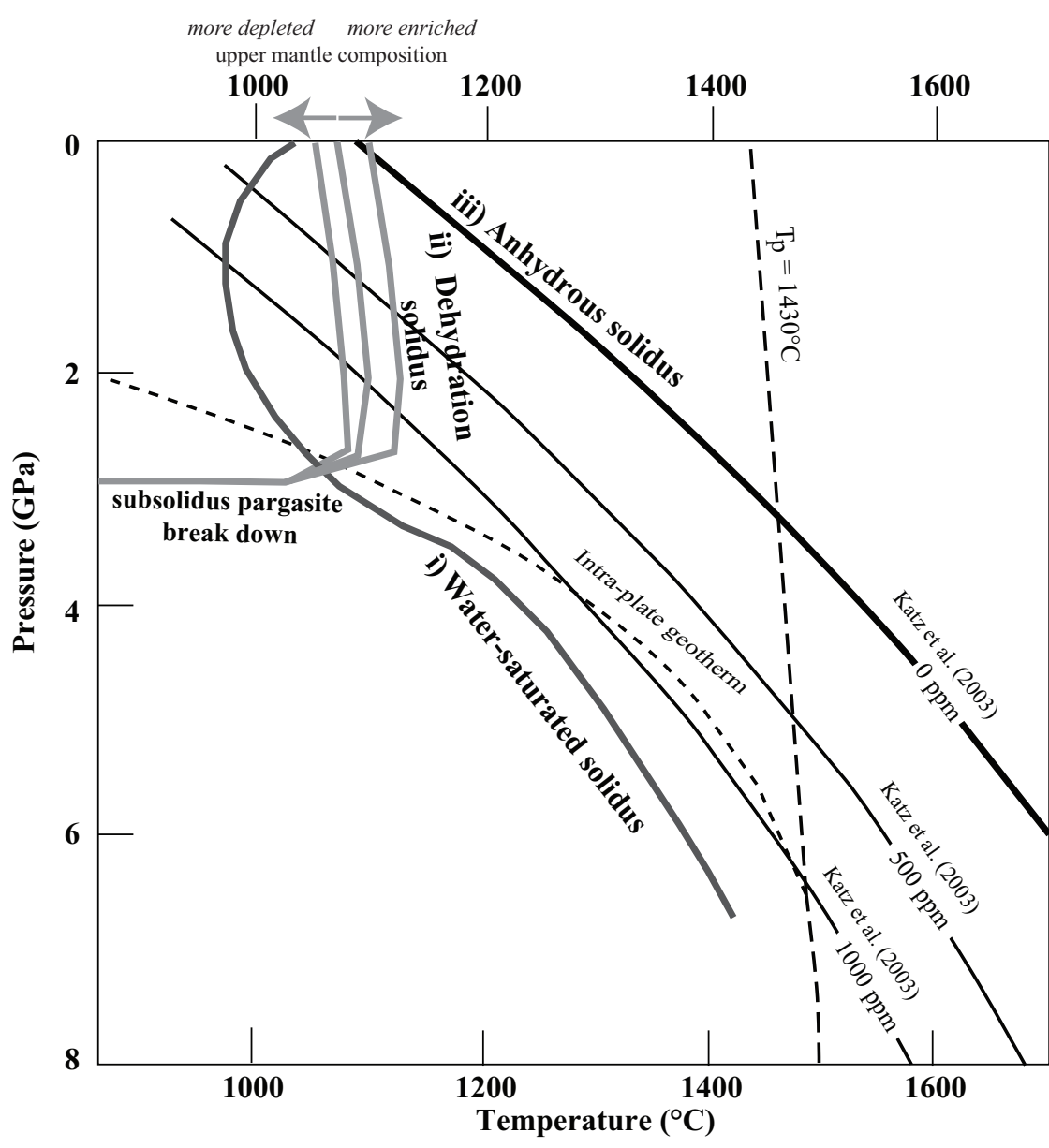


Fig.1.

Figure2

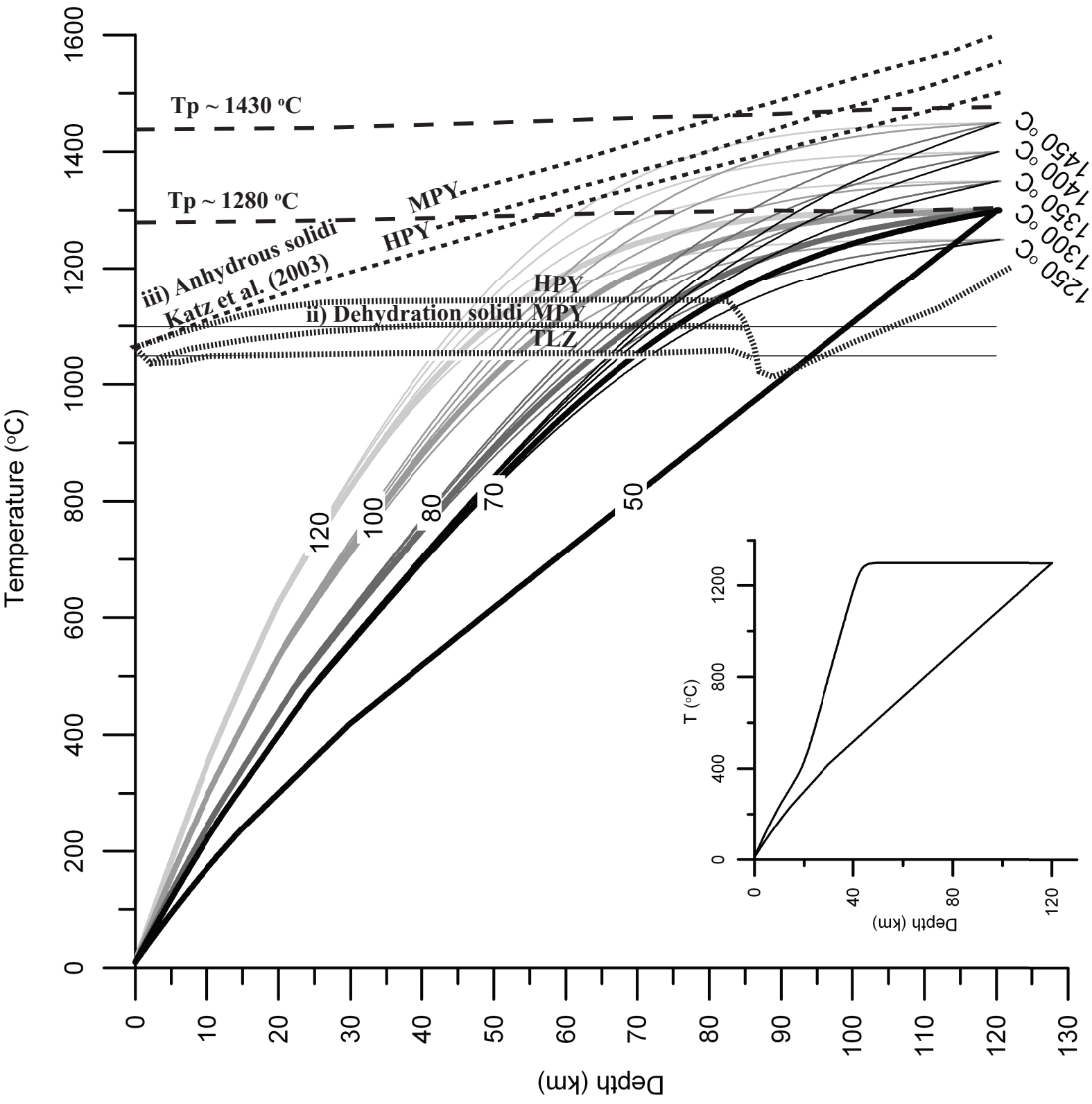


Fig.2.

Figure 3

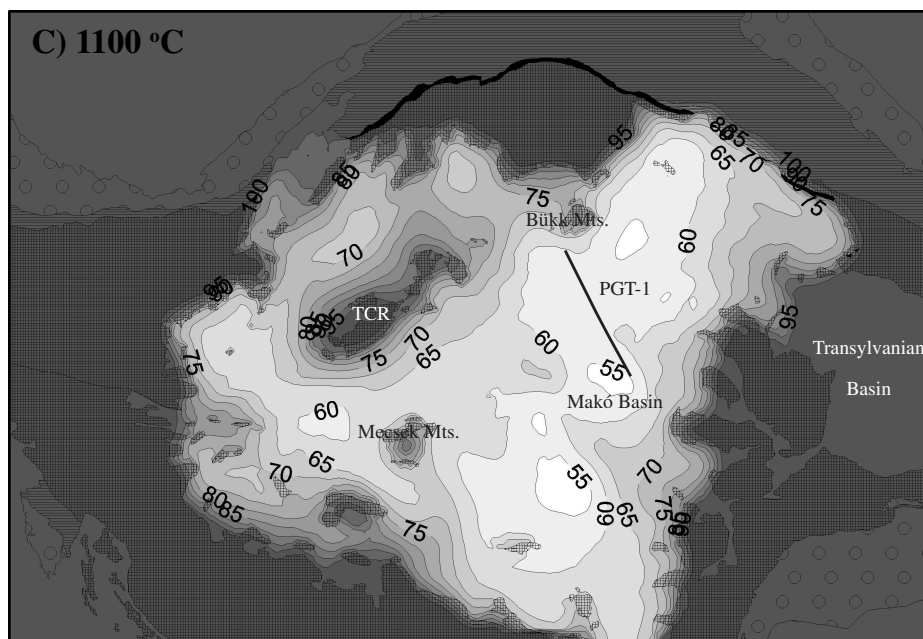
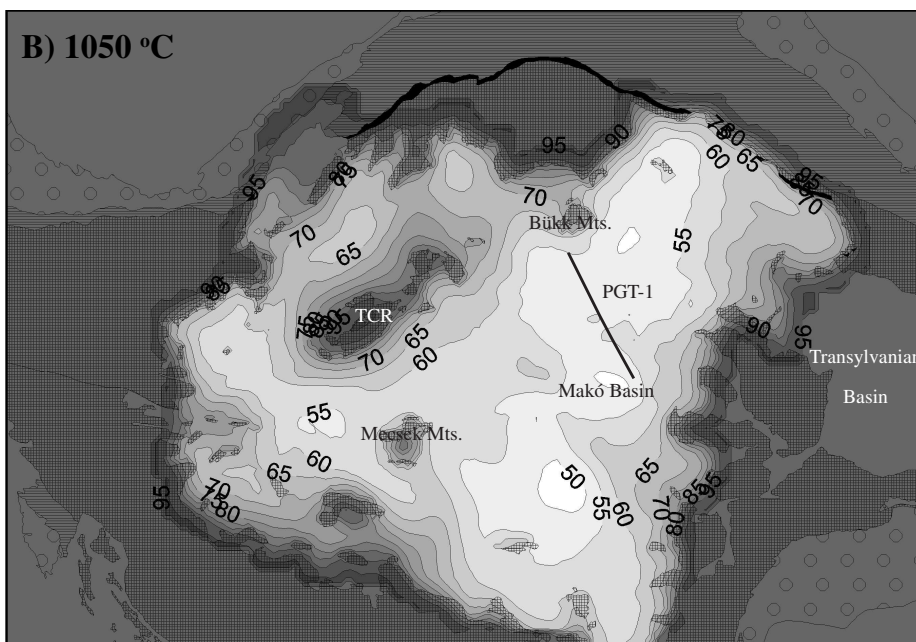
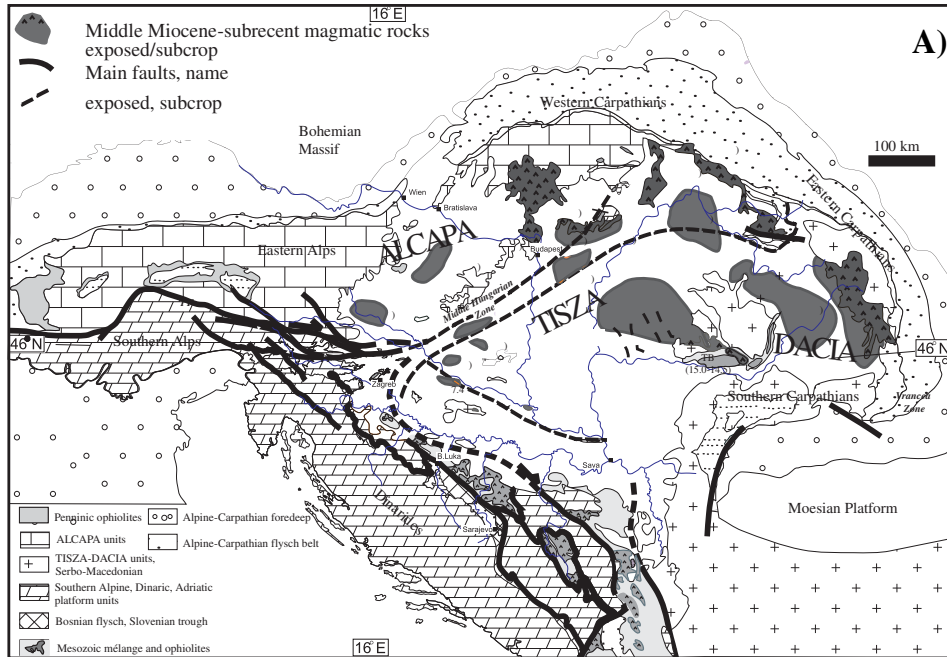


Fig. 3.

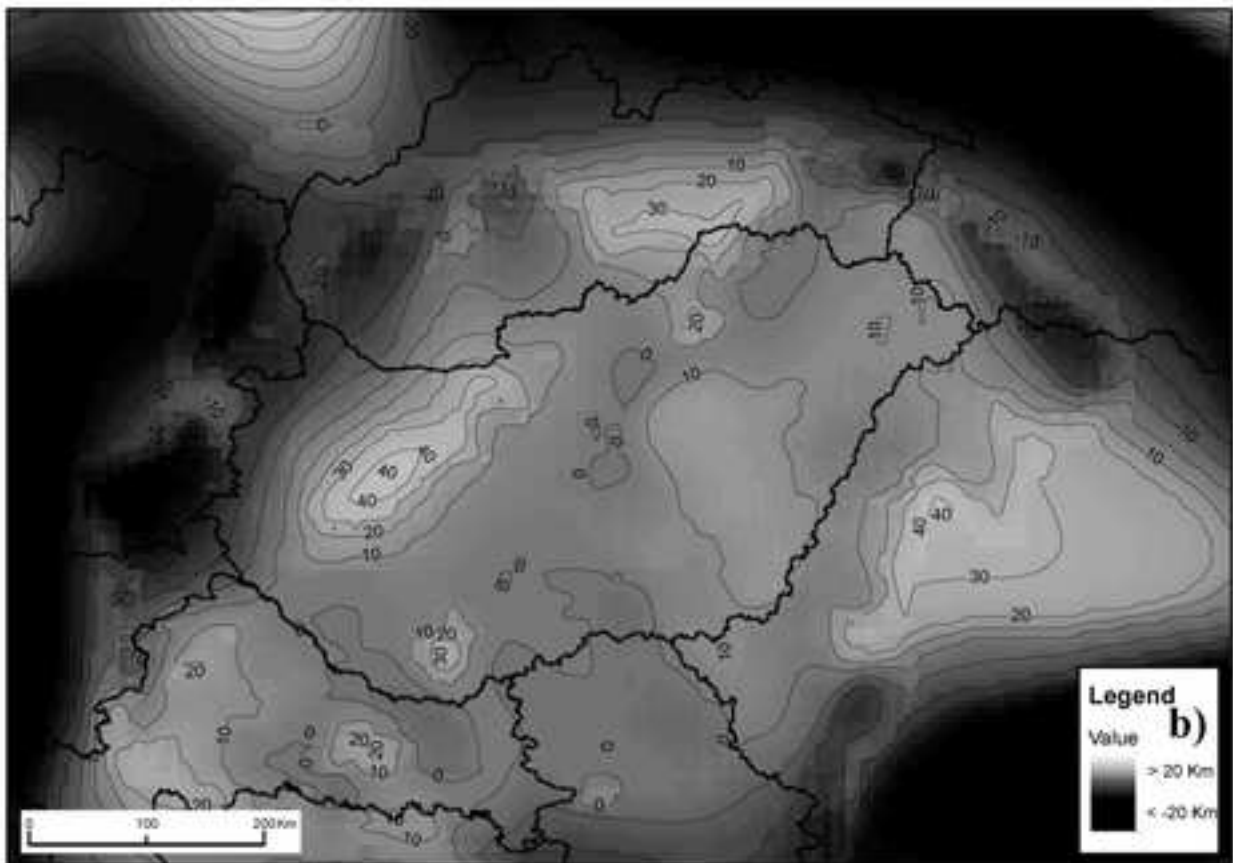
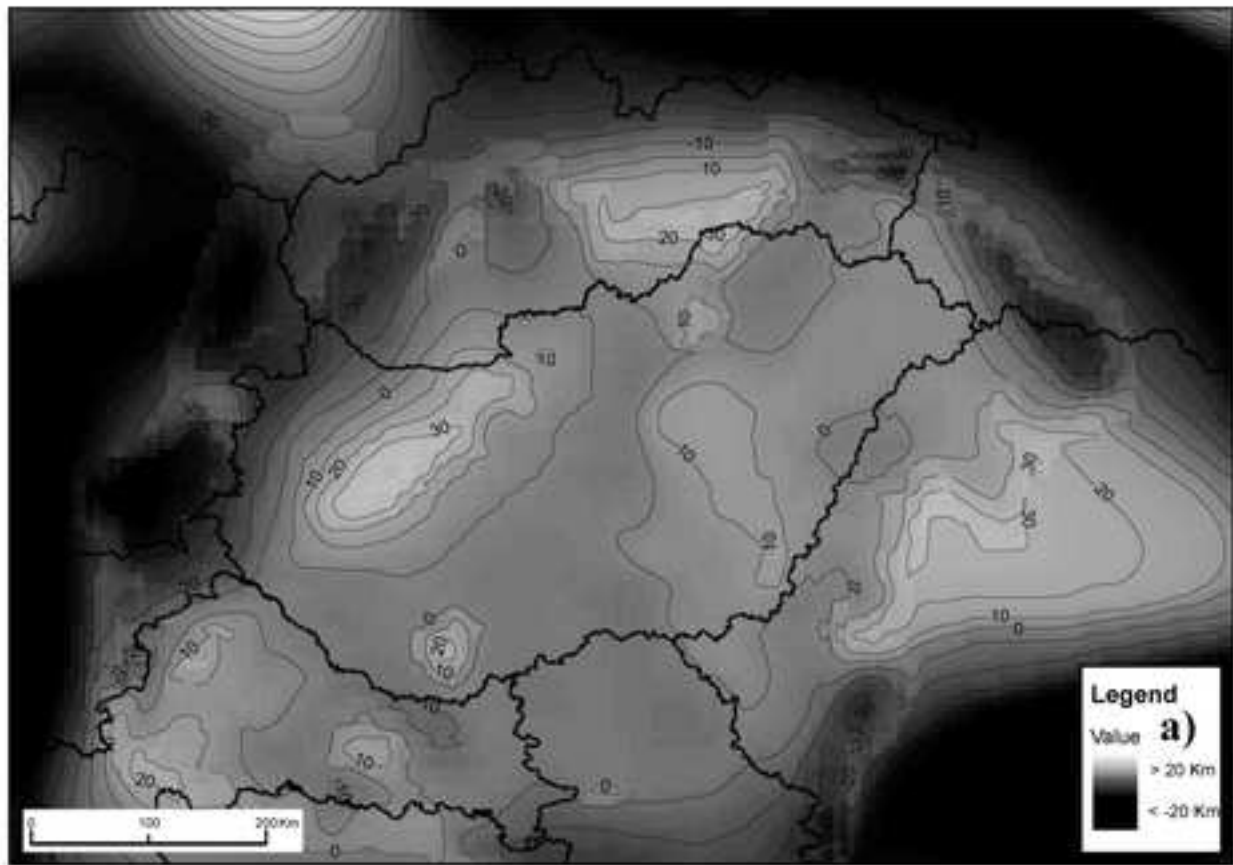


Fig. 4.

Parameter	Value
initial crustal thickness	35 km
initial lithospheric thickness	120 km
density of crust	2800 kg/m ³
density of mantle	3300 kg/m ³
temperature at the surface	10 °C
temperature at 120 km depth	1300 °C
thermal expansion coefficient	3.1 x 10 ⁻⁵ 1/°C
thermal diffusivity	7.8 x 10 ⁻⁷ m ² /s
heat production in the upper crust	8 x 10 ⁻⁷ W/m ³
thickness of the upper crust	15 km

Table 1.

Copyright Transfer Statement

Publisher: Akadémiai Kiadó Zrt., Budapest, Hungary

The Copyright Transfer Statement should be printed, signed, and uploaded to: <http://www.editorialmanager.com/AGGE/>

Author

Name:

Kovács István János

Address:

Geological and Geophysical Institute of Hungary, H-1143, Stefánia street 14.

E-mail address:

kovacs.istvan.janos@mfgi.hu

Article information

Title:

The role of pargasitic amphibole in the formation of major geophysical discontinuities in the shallow upper mantle

Journal title: Acta Geodaetica et Geophysica (formerly Acta Geodaetica et Geophysica Hungarica)

Co-authors:

László, Lenkey², David. H. Green³, Tamás, Fancsik¹, György, Falus¹, János Kiss¹, László, Orosz¹, Jolán Angyal¹, Zsuzsanna Viktor¹

I. Transfer of copyright

By execution of the present Statement Author transfers copyright and assigns exclusively to Publisher all rights, title and interest that Author may have (for the extent transferable) in and to the Article and any revisions or versions thereof, including but not limited to the sole right to print, publish and sell the Article worldwide in all languages and media. Transfer of the above rights is referred to as those of the final and published version of the Article but does not restrict Author to self-archive the preprint version of his/her paper (see Section III).

II. Rights and obligations of Publisher

The Publisher's rights to the Article shall especially include, but shall not be limited to:

- ability to publish an electronic version of the Article via the website of the publisher Akadémiai Kiadó, www.akademiai.com (in Hungary), as well as the co-publisher's website, <http://link.springer.com> (outside of Hungary) or any other electronic format or means of electronic distribution provided by or through Akadémiai Kiadó or Springer from time to time, selling the Article world-wide (through subscriptions, Pay-per-View, single archive sale, etc.)
- transforming to and selling the Article through any electronic format
- publishing the Article in the printed Journals as listed on the official Website of Publisher
- transferring the copyright and the right of use of the Article onto any third party
- translating the Article
- taking measures on behalf of the Author against infringement, inappropriate use of the Article, libel or plagiarism.

Publisher agrees to send the text of the Article to the e-mail address of Author indicated in the present Statement for review before the first publishing either in paper and/or electronic format (Proof). Author shall return the corrected text of the Article within 2 days to the Publisher. Author shall, however, not make any change to the content of the Article during the First Proof preview.

III. Rights and obligations of Author

The Author declares and warrants that he/she is the exclusive author of the Article - or has the right to represent all co-authors of the Article (see Section IV) - and has not granted any exclusive or non-exclusive right to the Article to any third party prior to the execution of the present Statement and has the right therefore to enter into the present Statement and entitle the Publisher the use of the Article subject to the present Statement. By executing the present Statement Author confirms that the Article is free of plagiarism, and that Author has exercised reasonable care to ensure that it is accurate and, to the best of Author's knowledge, does not contain anything which is libelous, or obscene, or infringes on anyone's copyright, right of privacy, or other rights. The Author expressly acknowledges and accepts that he/she shall be entitled to no royalty (or any other fee) related to any use of the Article subject to the present Statement. The Author further accepts that he/she will not be entitled to dispose of the copyright of the final, published version of the Article or make use of this version of the Article in any manner after the execution of the present Statement. The Author is entitled, however, to self-archive the preprint version of his/her manuscript. The preprint version is the Author's manuscript or the galley proof or the Author's manuscript along with the corrections made in the course of the peer review process. The Author's right to self-archive is irrespective of the format of the preprint (.doc, .tex, .pdf) version and self-archiving includes the free circulation of this file via e-mail or publication of this preprint on the Author's webpage or on the Author's institutional repository with open or restricted access. When self-archiving a paper the Author should clearly declare that the archived file is not the final published version of the paper, he/she should quote the correct citation and enclose a link to the published paper (<http://dx.doi.org/jDOI> of the Article without brackets]).

IV. Use of third party content as part of the Article

When not indicating any co-authors in the present Statement Author confirms that he/she is the exclusive author of the Article. When indicating coauthors in the present Statement Author declares and warrants that all co-authors have been listed and Author has the exclusive and unlimited right to represent all the co-authors of the Article and to enter into the present Statement on their behalf and as a consequence all declarations made by Author in the present Statement are made in the name of the co-authors as well. Author also confirms that he/she shall hold Publisher harmless of all third-party claims in connection to non-authorized use of the Article by Publisher. Should Author wish to reuse material sourced from third parties such as other copyright holders, publishers, authors, etc. as part of the Article, Author bears responsibility for acquiring and clearing of the third party permissions for such use before submitting the Article to the Publisher for acceptance. Author shall hold Publisher harmless from all third party claims in connection to the unauthorized use of any material under legal protection forming a part of the Article.

V. Other provisions

Subject to the present Statement the Article shall be deemed as first published within the Area of the Hungarian Republic. Therefore the provisions of the Hungarian law, especially the provisions of Act LXXVI of 1999 on Copy Rights shall apply to the rights of the Parties with respect to the Article. For any disputes arising from or in connection with the present Statement Parties agree in the exclusive competence of the Central District Court of Pest or the Capital Court of Budapest respectively.

Date and place of signature:

Monor, 02.06.20116.

Signature:

